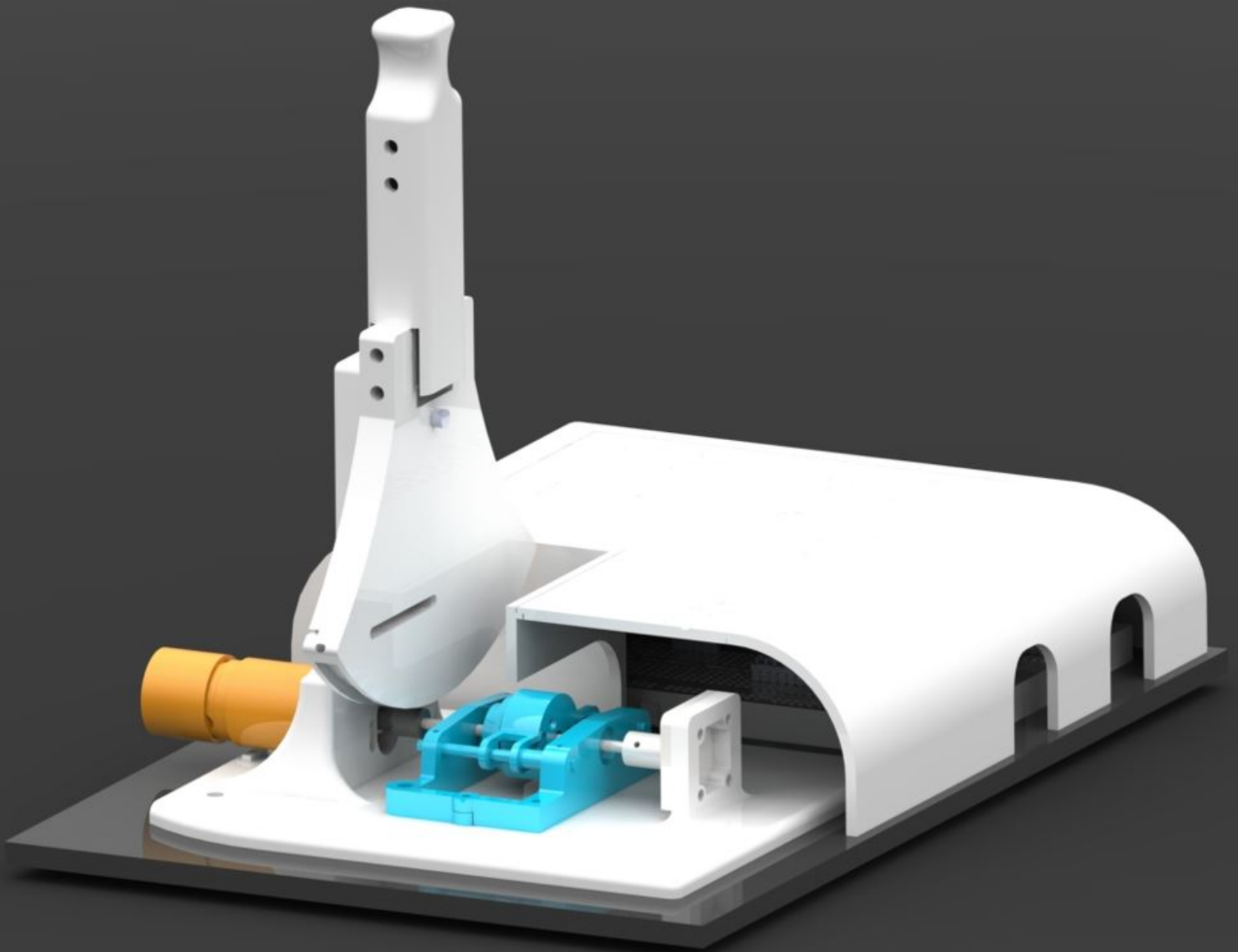


Developing hybrid force feedback: coupling **motors** and **brakes** can reduce the total actuator size and improve haptics quality

S.A. van Ginneken



Developing hybrid force feedback: coupling motors and brakes can reduce the total actuator size and improve haptics quality

by

S.A. van Ginneken

to obtain the degree of Master of Science
at the Delft University of Technology,
to be defended on August 24th 2022.

Student number:	4356934	
Project duration:	Sept 2021 - Aug 2022	
Thesis committee:	Prof. Dr. ir. D.A. Abbink	TU Delft, supervisor, chair
	Dr. M. Wiertlewski	TU Delft, daily supervisor
	J. Luijttten	SenseGlove, lient side daily supervisor
	Dr. C. Della Santina	TU Delft, external committee member

An electronic version of this thesis is available at <http://repository.tudelft.nl/>.

CONTENTS

1	Introduction	2
2	Theoretical Analysis of Hybrid Actuation	4
2.1	Hybrid Actuation	4
2.2	Kinematic breakdown	4
2.3	Simulation Model	5
3	Simulation Model Validation	6
3.1	Simulation Model Adjustments	6
3.2	Simulation Results	7
4	Prototype Design and Implementation	9
4.1	Hardware & Manufacturing	9
4.2	Software & Control	10
4.3	Simulation to Prototype comparison	12
5	Prototype Validation	13
5.1	Mechanical Rendering Ability	13
5.2	Human-in-the-loop Validation	14
5.3	Experiment Results	15
5.4	Survey, 5-point Likert scale	18
6	Discussion	18
6.1	Simulation Model	18
6.2	Prototype	18
6.3	Reflection on Literature	19
7	Conclusions	20
	References	20
	Appendix A: Calculation of Weight Benefit	22
	Appendix B: Hybrid Actuator Force Discrepancy	23
	Appendix C: Supplementary Documents	24
	C.1 Collection of Code	24
	C.2 Electrical Components	24
	Appendix D: Prototype Actuator Characteristics	25
	Appendix E: Control Sequence	26
	Appendix F: Simulation Results	27
	Appendix G: Experiment Results	29

Developing hybrid force feedback: coupling brakes and motors can reduce the total actuator size and improve haptics quality

S. A. van Ginneken

Abstract— Hand-worn haptic systems must be able to produce high-quality haptics while also being lightweight and energy-efficient. In order to meet market expectations, research is being done into novel drivetrains that may be implemented in hand worn devices. This is being pushed forward by the growing demand in the virtual reality sector, which is placing pressure on the development of new wearable force feedback technology. In order to validate a proof of concept, this thesis proposes a novel force feedback drivetrain with a dual actuator setup—a motor and a brake—that is integrated into a tabletop prototype. Using both a motor and a brake will reduce weight and improve the haptic rendering quality relative to each component when considered separately.

To evaluate the presumptive advantages, a theoretical analysis into the suggested hybrid actuation solution is conducted. The analysis comprises of numerous simulations using a model of the hybrid drivetrain's working principle. Additionally, the analysis is employed to investigate and spot any early-stage defects or undesirable behavior. Consequently, a 3D model was created in order to 3D print a functioning prototype in order to apply the theory in a physical version. The prototype is initially used to validate the simulation model and enforce the findings of the theoretical analysis. Force data is measured when using the prototype and in turn is fed into the simulation model to assess whether the output behaviour is consistent with the prototype. Both the model's competence and the prototype's predictability are assessed using the outcomes.

Finally, an experiment is conducted to both assess the mechanical performance and predictability as well as the participant's perception; 2 virtual environments and 3 actuation modes (motor, brake, and hybrid) were cross-examined and each repeated 6 times, for a total of 36 trials. This experiment ultimately assesses the prototypes validity and determines whether the theoretically assumed benefits are present in the prototype as well. Finally, the participant completes a questionnaire in the form of a 5-point Likert scale to determine if the experiment data complies with the users experience.

The theoretical analysis revealed both reliable behavior and potential problems, such as oscillations in feedback force due to rapid switching between actuator activity. However, the cause of this behaviour was identified and anticipated to be less pronounced during use of the prototype. The prototype was successfully designed and produced, and a comparison to the model revealed consistent findings and, thus, predictable behavior. However, the model occasionally miscalculated the velocity. The experiment also shows that the hybrid drivetrain approach is promising and outperforms the state of the art both in mechanical prowess as well as physical fidelity when providing haptic feedback; the motor fails to render rigid objects and the brake cannot render spring-like objects, while the hybrid approach can render both successfully.

The thesis demonstrates that additional investigation into the suggested drivetrain is supported, despite some obvious limitations. When compared to equally powerful DC motors, the hybrid technique, as employed in the prototype, is capable of portraying the largest variety of haptics, including hard walls, impacts, and stiffness while potentially conserving weight.

finger haptics, hybrid actuation, wearable haptics



1 INTRODUCTION

Virtual Reality, or VR, is becoming more and more ingrained in modern technology. gaining ground in numerous industries, including 1. health care, where it is employed as a gamification- and training tool for high-risk procedures like surgery [1]; 2. military, where it is primarily used as a gamification- and training tool for high-risk situations [2]; and 3. gaming and teleoperation [3]. The primary reason is due to closely replicating reality and immediately activating the human sense of sight through the use of VR goggles, VR gives an immersive experience.

The usage of VR is expanding, and this is accelerating related technology advancements, including methods of control. It is now possible to record hand and finger motions and use them as a mode of control, as opposed to the past where characters in a virtual environment were controlled by physical gaming controllers. Pair this with high quality haptics and it is possible to use your hands to grasp, feel

and interact with a virtual environment.

Increased control accuracy, physical fidelity, and immersion are just a few benefits that haptics can provide. Great examples indicating this value are VR-ready force feedback gloves such as the Nova from SenseGlove [4], the Da Vinci robot by Intuitive Surgical [5], robots on MARS operating with huge latency [6]. The first of which enables this mentioned ability to grasp, feel and interact with a virtual environment. However, challenges arise when trying to achieve high quality haptics like the rendering of squishy objects or sudden impacts. The market requires light, wearable tech that can produce high-quality haptics, yet the most advanced solutions find it difficult to meet all of these requirements.

To generate high quality haptics in VR environments, gloves are the go-to solution as they build upon a humans inherently intuitive means of control and sensing: the hands. Literature puts forward multiple of such haptic feedback gloves, ranging from simple gloves like; the pneumatic

palm-based Rutgers Master II [7] which offers great force to weight ratio at the cost of wearability and range-of-motion, the binary palm-based Wolverine [8] which offers great force but very limited haptic rendering range due to being unidirectional and limited to a on or off state, and the J-Glove [9], to complex data gloves; among others the SAFE glove [10], the Hexotrac [11] or the commercially available actively motor powered CyberGrasp [12] where achieving high quality haptics comes at the cost of adding more weight and not being wireless; the Cybergrasp weighs over 450 grams without the needed glove. In contrast, the fully passively brake powered SenseGlove Nova weighs 320 grams in total which is still heavy compared to the earlier mentioned simple gloves, however it includes encoders, transmitters, controller boards and is fully wireless. The range of gloves again clearly indicates the challenges of wearable and wireless haptics, these challenges often dictate a choice between active or passive actuation. Active devices can generally render a vast range of haptic sensations, is heavy and weak, whereas passive devices have limited haptic capabilities, but in turn are light and strong.

The terms active and passive are presented in literature as typical types of actuation to generate force feedback. Wang et al. 2019 [13] defines these within the glove-type haptic systems as;

- *"Active actuation: The active force feedback gloves can provide not only active motion, but also resistance force or torque."*
- *"Passive actuation: The passive gloves use a brake, controllable damper or electromagnetic clutch to provide a resistance force."*

In a more general sense; passive actuation can only dissipate energy from a system (resist a force input) making the system inherently safe as it can never exert a force on the user, even in failure. In addition to dissipating energy, active actuation can also add energy to a system (enhance a force input). In order to still maintain safety, generally a maximum output force of 10N per finger is set [13].

Due to being active and continually working, active actuation methods [10][11] are capable of rendering more complex haptics such as stiffness, but typically use more power to generate similar magnitudes of force than passive solutions [8][4]. These passive solutions are light and strong, however their use is limited since they can only resist an input force; generate a force opposing that of the input. Since passive actuators are strong, actuators like brakes can generate some unique haptics such as interaction with rigid objects, such as walls.

Passive actuation is used in force feedback gloves like the Senseglove Nova [4] because it is secure, lightweight, effective, and capable of realizing a variety of feedback forces. However, because the glove is only capable of offering passive force input, it is not possible to represent items with low stiffness, such as a sponge. SenseGlove is looking for a solution which boosts the rendering capabilities of their gloves in order to build an even more complete product. This thesis aims to offer SenseGlove a creative solution while also offering academically solid knowledge.

The use of active rather than passive actuation, as in the CyberGrasp [14], is a commonly used remedy. However,

these alternatives are heavier, which reduces wearability, is less efficient, and ultimately unable to render rigid object interaction. Active actuation therefor fails to offer a holistic solution to the mentioned challenges:

- High quality haptics demands active actuation; heavy when adequate
- Lightweight demands passive actuation; limited usability when adequate
- Wireless functionality demands energy efficiency; low energy usage means low force output

Literature lacks a hybrid solution which combines the two actuation methods, passive and active, to compensate each others drawbacks by making use of their individual strengths. In order to close this gap, this thesis proposes a hybrid actuated drivetrain that can be used in wearable haptic solutions. The topic of this thesis reflect the goal;

Developing hybrid force feedback: coupling motors and brakes can reduce the total actuator size and improve haptics quality

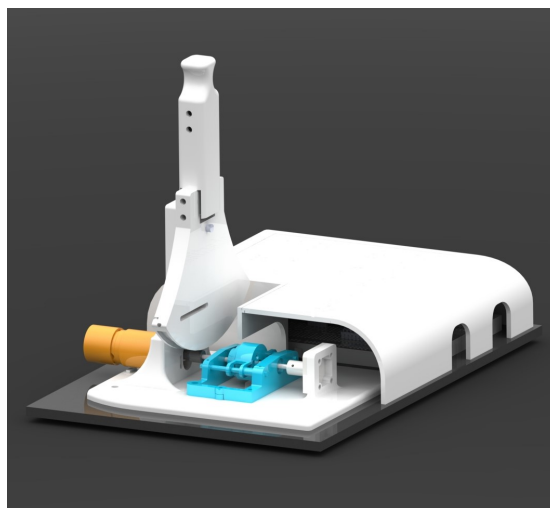


Fig. (1) Render of the proposed hybrid drivetrain consisting of a motor, orange, and a brake, cyan, working together in order to generate high quality haptics while reducing weight

The objective of this thesis is to develop a drivetrain that can produce high-quality haptics while reducing size and weight. See fig 1 for a visual representation of the proposed drivetrain embedded into a tabletop prototype. In comparison to active or passive actuation systems, combining the two enables the production of higher quality haptics, including rigid object and low stiffness interaction, while staying lightweight and small to be integrated into wearable devices like haptic gloves. Increasing the haptic quality capability of wearable devices will increase their application potential and ultimately conform to the market demands

The thesis proposes the hybrid solution by the means of the following sections;

- Theoretical Analysis of Hybrid Actuation
- Simulation Model Validation
- Prototype Design and Implementation
- Prototype Validation

The first introduces the proposed principle, the second validates the created model, the third describes the implementation of the principle into a prototype and the last validates the prototype. The results of the validation are discussed in the *Discussion*, which is followed by the *Conclusion* and an appendix.

2 THEORETICAL ANALYSIS OF HYBRID ACTUATION

A theoretical analysis of the proposed hybrid actuation solution is carried out to assess the presumed advantages. Through kinematic breakdown and simulations, the underlying theory pertaining to this hybrid actuation approach is carefully explained and analyzed in order to obtain insight into the behavior of the drivetrain and identify potential pitfalls and issues at an early stage. These are then assessed, and when appropriate, solutions are developed and put into practice. A successful and effective design process depends on this. It must be remembered, nevertheless, that simulations and theories are less complex and therefore less nuanced than reality.

2.1 Hybrid Actuation

As already touched in the *Introduction*, passive and active actuation both have clear advantages and drawbacks, the most important ones are listed in table 1:

Combining these two types of actuation into a new "Hybrid" actuation technique might, in principle, alleviate the shortcomings of both actuation techniques. In this thesis, existing and proven actuation devices are chosen to build the novel hybrid drivetrain. This way, the device can also be operated by just one of the actuators to recreate a fully passive or active system, enabling the comparison between the three. The passive device is the electromagnetic brake found in the SenseGlove Nova [4]; see figure 2. The active device is the Faulhaber 2342S048C, as depicted in fig 3, which is a DC motor working at a maximum of 48V. The hybrid drivetrain employs both actuators, but runs the DC motor on a lower voltage to imitate a smaller motor with approximately one-fourth the torque. In addition, as a part of the research objective, the new "hybrid" approach cannot be heavier than a suitable active actuation device.



Fig. (2) SenseGlove proprietary electromagnetic brake



Fig. (3) Faulhaber 2342S048C [15]

In theory, the mimicked smaller DC motor could have a volume which is 6 times smaller than the Faulhaber 2342S048C, see appendix A for the relevant theory. As built, the Faulhaber motor weighs 88 grams. While the brake weighs only 27 grams. In theory, the hybrid setup with an actual smaller motor could weigh 42 grams ($27 + 88/6 = 42$) which is significantly less than the full-sized Faulhaber motor.

A big disadvantage of using a smaller motor is that there will be a big discrepancy between the maximum forces generated by the brake and the small DC motor (see appendix B). Exact values are measured when the actual prototype is built. To evaluate the presumptive advantages, a theoretical analysis into the suggested hybrid actuation solution is conducted.

2.2 Kinematic breakdown

In order to be able to analyse the drivetrain, a model to run simulations has to be created. In turn, to create a representative model, a proper kinematic representation of the hybrid drivetrain is created, and presented in this section.

A single mass-spring-damper system is used to represent the drivetrain, it is chosen to take only one dimension into account to reduce complexity. This mass-spring-damper system is used to imitate the hybrid drivetrain, which in turn renders objects such as springs and sponges. In actuality, when you compress and decompress an object like a spring, your finger deforms; the tissue surrounding the bone is compressed and decompressed. In order to determine whether or not it has any effect, a second mass-spring-damper system is added. In order to reduce the complexity of the model and place emphasis on the interaction between the actuators and the introduced finger dynamics, gravity and friction are excluded.

Fig 4 on the next page shows the combined mass-spring-damper system and the corresponding forces in equations 1-2. In these equations, F_{O_1} is the actuator force during compression, F_{O_2} the actuator force during decompression or maintaining compression. Lastly, F_f is the force generated by the compression of the finger. Fig 5 on the following page shows the free body diagrams of the two masses, corresponding to the virtual object and the finger, together with the corresponding equilibria in equations 3 and 4.

$$F_{O_{1,2}} = -K_O * (x_1 - L_{O_0}) - B_O * \dot{x}_1 \quad (1)$$

$$\max(F_{O_2}) = \max(F_{O_1})/4$$

$$F_F = -K_F * ((x_2 - x_1) - L_{F_0}) - B_F * (\dot{x}_2 - \dot{x}_1) \quad (2)$$

Passive		Active	
Pros	Cons	Pros	Cons
High force to energy consumption ratio	Only resistive forces	Easy to control	Low force to energy consumption ratio
Lightweight	Can not render stiffness	Can resist and amplify	Heavy
Safe			Unsafe/weak trade off
			Can not render infinite stiffness

TABLE (1) General Pros and Cons of Active and Passive actuation methods

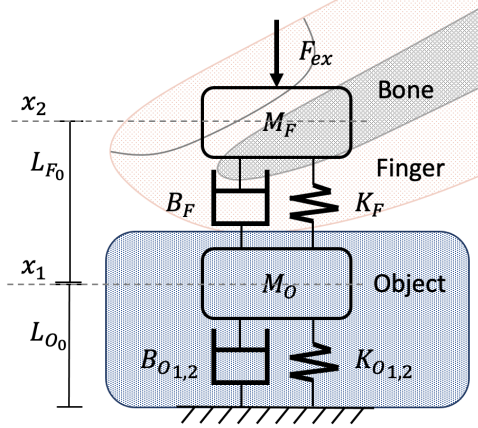


Fig. (4) Schematic drawing of the modelled system

$$M_O * \ddot{x}_1 = F_{O,1,2} - F_F \quad (3)$$

$$M_F * \ddot{x}_2 = F_F - F_{ex} \quad (4)$$

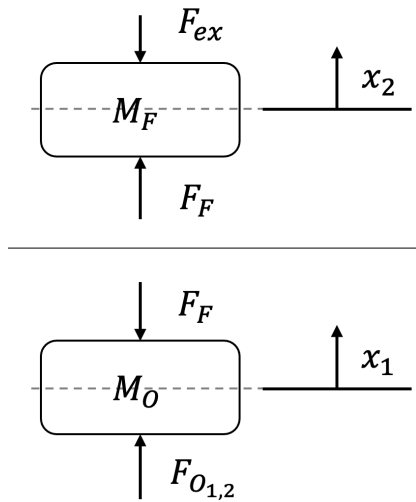


Fig. (5) Free Body Diagrams of the modelled system

Despite being depicted as blocks, the masses represent point masses and the variables used are compiled in the table 2 alongside their definitions.

As previously indicated, the hypothetical hybrid drivetrain is comprised of a DC motor and an electromagnetic brake. Since the brake is more potent and more efficient at delivering force, it is utilized for all resistive actions; force opposes movement direction. The DC motor is only triggered when a force is required that cannot be created by the brakes; an active force, such as the force a spring exerts

Param	Definition
M_O	Mass of the object (spring)
M_F	Mass of the finger
K_O	Spring stiffness during compression
B_O	Object damping coefficient during compression
K_F	Spring stiffness of finger
B_F	Damping coefficient of the finger
$L_{O,0}$	Length of the object "spring" in rest
$L_{F,0}$	Length of the finger "spring" in rest
T	Time length of the simulation
h	Step size used in the simulation
F_{ex}	User input force

TABLE (2) Simulation parameters and their definitions

on your finger when you decompress it. In essence; when compressing the virtual object, the brake is engaged; $\dot{x}_1 < 0$, whereas the DC motor is engaged when decompressing or maintaining compression of the virtual object; $\dot{x}_1 > 0$. Where x_1 and \dot{x}_1 represent the mass's, M_O , position and velocity respectively; see fig 5. In the simulation model a force ratio between the maximum actuator output of 1:4, motor:brake, is used.

2.3 Simulation Model

The above kinematics are fully adopted into a model; all parameters and force equations are included in the model. In order to run simulations of the model a control sequence is chosen, this control sequence dictates the inputs and outputs of the model and whether the system is closed or open loop. There can be a vast difference between the results depending on the type of control, especially in models which are composed of non-linear systems, like the hybrid drivetrain principle, as these can be unpredictable due to their non-linear relation between input and output.

A choice between force-control and displacement-control has to be made, these are straight forward means of control suitable for the proposed model. The diagrams 6 on the following page and 7 on the next page show the different control loops. In these diagrams, EOM stands for Equations Of Motion and RK4 signifies the iteration step, which is done using standard Runge Kutta 4 due to the great balance between cost and accuracy, cost however is not computed or taken into account due to the simplicity and goal of using the model as well as time restrictions.

Fig 7 on the following page reveals that in this case, evaluating what happens during displacement control is not relevant; the inputs correlate directly to the outputs via the EOM, resulting in a very predictable output force curve, given the input displacement curve. However, fig 6 on the next page shows that the output forces, $F_{O,1,2}$ and F_f , of the current time step are both dependent on the user input force,

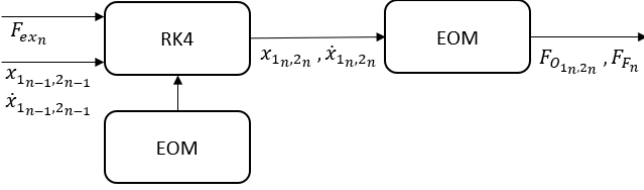


Fig. (6) Force-control diagram



Fig. (7) Displacement-control diagram

F_{ex_n} , the displacements, $x_{1,2}$, and velocities, $\dot{x}_{1,2}$, of the previous time step. Depending on the system parameters and inputs, given the non-linearity of the hybrid system, unpredictable behaviour can be expected.

3 SIMULATION MODEL VALIDATION

Multiple simulations are ran with different functions for F_{ex} ; a repeating step input (5), a repeating ramp function (6) and lastly a sinus (7). In these functions, t is the time step within the simulation of length T and step size h . Furthermore, the variable a can be varied to change the magnitude of the force input. The graphs in fig 8 correspond to each mentioned equation relatively. The parameters regarding the object, M_O , K_O , and B_O , are chosen to represent a fictional compression spring with a mass of 5 grams and a stiffness of 4 N/rad. Damping can generally only be determined experimentally, and therefore, this parameter is optimised by trial and error during running various simulations.

$$F_{ex} = \begin{cases} 2 * a & t = [0, \frac{T}{4}] \cup [\frac{T}{2}, \frac{3T}{4}] \\ 0 & t = [\frac{T}{4}, \frac{T}{2}] \cup [\frac{3T}{4}, T] \end{cases} \quad (5)$$

$$F_{ex} = \begin{cases} 2 * a * \frac{4*t}{T} & t = [0, \frac{T}{4}] \\ 2 * a + 2 * a * (1 - \frac{4*t}{T}) & t = [\frac{T}{4}, \frac{T}{2}] \\ 2 * a * (\frac{4*t}{T} - 2) & t = [\frac{T}{2}, \frac{3T}{4}] \\ 2 * a + 2 * a * (3 - \frac{4*t}{T}) & t = [\frac{3T}{4}, T] \end{cases} \quad (6)$$

$$F_{ex} = a * \sin(t * -0.5 * \pi) - (a) \quad t = [0, T] \quad (7)$$

As it is beyond the scope of this thesis to perform a study towards reliable finger parameters, M_F , K_F and B_F are taken from a study by Bi Q et al [16]. Bi Q presents three different values for the mass, stiffness, and damping coefficient of the fingertip corresponding to three different postures; flexion, half-flexion, and extension. Half-flexion is the posture in which a human naturally would compress a spring which sits on a flat surface. As such, these values were adopted;

- $K_f = 584.6 \text{ N/m}$

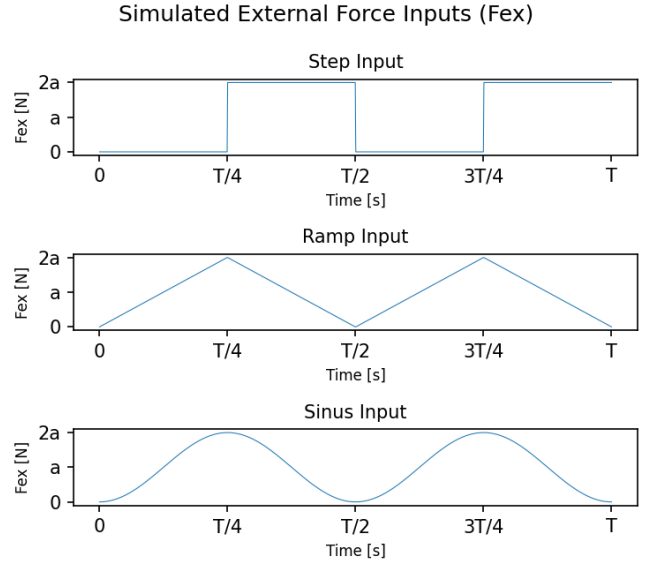


Fig. (8) Overview of the three input curves

- $B_f = 1.53 \text{ kg/s}$
- $M_f = 2.1 \times 10^{-2} \text{ kg}$

Take into account that these values can vary significantly between humans. As such, the results found with these values should only be understood as indicative. Lastly, the value for L_{F_0} is determined by measuring the compression of the researcher's fingertip when pressing it on a flat surface.

From the evaluation of the mentioned simulations, the behaviour of the conceptual hybrid drivetrain can be estimated, giving insight into the possibilities, limitations, and potential pitfalls. Enabling the addressing of unwanted behaviour and challenges before running into them during implementation or experiments.

3.1 Simulation Model Adjustments

In 4, the design of the prototype is brought forward. This design will feature an end effector that rotates as opposed to translates. The simulation model is adjusted accordingly to adopt this change. Due to this change, and to keep the model from becoming too complex, the virtual object is changed to reflect a torsion spring rather than a linear compression spring.

Figure 20 on page 11 shows a simplified schematic overview of the realised prototype presented in the previous section. $T_{m,b}$ are the torques generated by the brake and the motor on the driveshaft, which in turn drives the end effector via the capstan transmission, indicated by the light grey block. F_{ex} is an indication of the force the user will exert on the device.

Figure 21 on page 12 is a visualisation which helps to contextualise the changes on different levels. The figure shows the connection between the new virtual situation, the new kinematic model, and the prototype that has been built.

Figure 9 on the next page shows the kinematic model separately. From this model, in conjunction with the new free body diagrams (fig 10 on the following page), the new equations of motion are derived, 8-11. The actuator

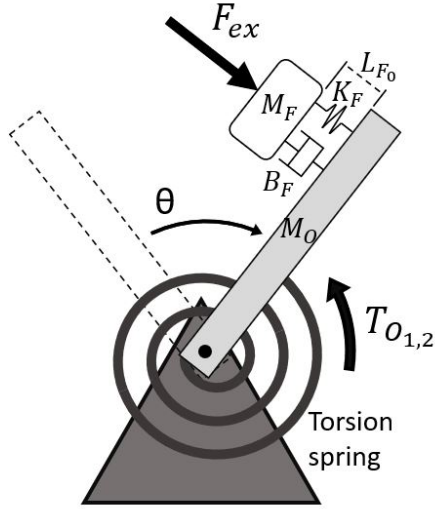


Fig. (9) Representation of the new kinematic model corresponding to the realised prototype

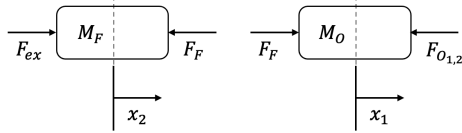


Fig. (10) Free body diagrams of the new system corresponding to the realised prototype

generated forces are now indicated as torque T_O due to the change from linear displacement to angular rotation. As such the only change is that the actuator forces $F_{O_{1,2}}$ are now dependent on angular rotation θ and velocity $\dot{\theta}$ instead of linear displacement and velocity, where θ is 0 whenever the end effector is in the upwards vertical position. The finger force F_f in eq 9 is calculated using an x-axis which is always perpendicular to the beam, see fig 9, and as such rotates with the rotation of the system. This causes the change that x_1 is no longer present in the equation, i.e. x_1 is always 0.

For the model it is assumed that the user exerted force F_{ex} is always perpendicular to the beam and coincident with F_f .

$$\begin{aligned} F_{O_{1,2}} &= T_O/L = -K_O \cdot \Theta - B_O \cdot \dot{\Theta} \\ \max(F_{O_2}) &= \max(F_{Motor}) \\ \max(F_{O_1}) &= \max(F_{Brake}) \end{aligned} \quad (8)$$

$$\begin{aligned} F_F &= -K_F * (x_2) - B_F * (\dot{x}_2) \\ \max(x_2) &= L_{F_0} \end{aligned} \quad (9)$$

$$\begin{aligned} M_O * \ddot{x}_1 &= F_{O_{1,2}} - F_F \\ \ddot{x}_1 &= \ddot{\theta} * L \end{aligned} \quad (10)$$

$$M_F * \ddot{x}_2 = F_F + F_{ex} \quad (11)$$

With the new model equations, the model parameters can be updated. Table 3 shows the updated parameter values. The mass M_O is set to 5grams to resemble a steel spring. The damping coefficient B_O as mentioned, has been

obtained by trial and error, by focusing on generating predictable model behaviour.

3.2 Simulation Results

As previously stated, the model was fed three distinct input curves for the external input force, F_{ex} . However, only the sinusoidal and step inputs are displayed in this section; the ramp input is included in appendix F as it does not offer further qualitative value. Fig 11 on the following page shows the input force, joined by the actuator output forces for brake and motor. The figure includes two graphs: one that plots these forces against the angular displacement θ and one that depicts the external input force, F_{ex} , in time. Find the initial values used below:

- $\theta_0 = -45 \text{ deg}$
- $x_2 = 0 \text{ deg/s}$
- $\dot{\theta}_0 = -45 \text{ deg}$
- $\dot{x}_2 = 0 \text{ deg/s}$

When plotting force displacement curves of ideal springs, usually their relation is linear and therefore a straight diagonal line. However, due to the force discrepancy between the actuators, the forces during compression and decompression are not continuous but non-linear and cause a discrepancy between the lines belonging to each movement direction, this is further explained in appendix B. The reason for the curves not being sharp when switching motion direction is due to the presence of mass and damping which cause delays in the behaviour which is expected. As such, the general shape of the External Force to Displacement curve is as expected.

It can be observed that the "Finger Tissue" force is perfectly aligned to the "External Force". This can be explained by the fact that the finger tissue is never completely compressed and therefore will always create a force equal to that compressing it. The "Motor" and "Brake" forces are correctly opposed to the external force. As expected there is a discrepancy between the maximum forces exerted by the brake and the motor, observable in the graph between an angle of 10 and 17 deg, however the forces oscillate heavily. This behaviour can be explained by the fact that the direction of movement keeps switching, and therefore the actuators in turn switch activity every time the movement direction switches. Due to the angular displacement at that point, the force discrepancy between the two actuators is large; the brake is strong enough to bring the velocity to 0, activating the motor which is not strong enough to generate the force needed to hold the current compression of the virtual spring; the end effector therefore gains velocity because of the input force being larger than the force output of the motor and compresses the virtual spring again, causing the brake to activate again and bring the velocity to 0, completing the circle which is the cause of the oscillations. This keeps happening until the input force is equal to the maximum force the motor can generate and therefore maintain compression of the virtual spring.

This behaviour occurs due to the external force being preset with respect to time, in this particular instance, a sinus curve. In reality, this does not necessarily happen; a human might be able to adapt to what he perceives as

Param	Value	Definition
M_O	0.005 kg	Mass of the object (spring)
M_F	2.1×10^{-2} kg	Mass of the finger
K_O	4 N/rad	Spring stiffness during compression
B_O	$1 \frac{\text{N}\cdot\text{s}}{\text{rad}}$	Damping coefficient of the object during compression
K_F	584.6 N/m	Spring stiffness of finger
B_F	1.53 kg/s	Damping coefficient of the finger
L_{F0}	6 mm	Length of the finger "spring" in rest
T	4 s	Time length of the simulation
h	8.3 ms	Step size used in the simulation
F_{ex}	varying N	User input force
θ_{min}	-45 deg	Minimum angle due to physical limitation
θ_{max}	45 deg	Maximum angle due to physical limitation

TABLE (3) Updated simulation parameters and their definitions

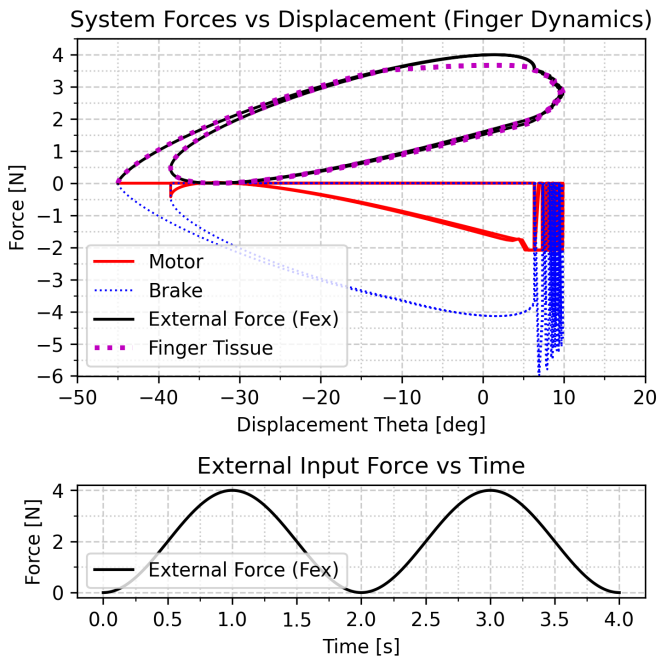


Fig. (11) Two plots visualise the behaviour of the model responding to the "External Force" input given in the bottom plot. The top plot shows the actuator forces together with the external force and the "Finger Tissue" force plotted against the displacement. To demonstrate how closely they are related, the finger forces are plotted in the same quadrant as the external force. The only difference being that the finger force flattens out close to 4 N as the finger is fully pressed.

resistance or spring force. This adaption might cause the force discrepancy to have less effect on the behavioural outcome. If the external input force dropped more drastically, the oscillatory behaviour would be reduced or even stopped altogether, see figure 33. To assess what would happen in reality, which means having a human in the loop, tests need to be conducted on a prototype to investigate whether the behaviour in the simulation accurately depicts real-life interaction using a hybrid drivetrain.

Furthermore, the same simulations were also carried out without finger dynamics inclusion and resulted in almost identical figures when the input force has no sudden

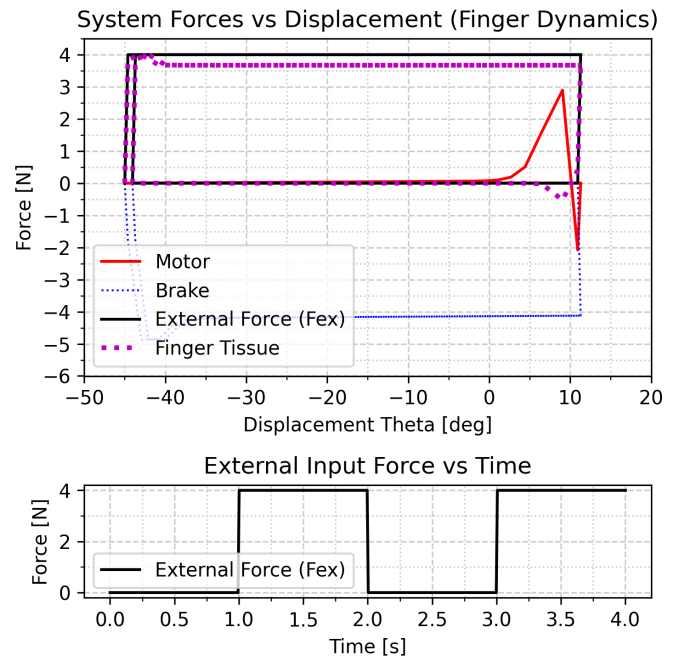


Fig. (12) Two plots visualizing the behaviour of the model responding to the "External Force" input given in the bottom plot. The top plot shows the actuator forces together with the external force and the "Finger Tissue" force plotted against the displacement. The finger forces are plotted in the same quadrant as the external force to show their differences better. The observed spikes in the "Finger Tissue" force are due to the sudden force changes in the "External Force"

changes, like the Ramp and Sinusoidal force inputs. However, when force inputs have sudden changes in magnitude, the difference is apparent. Further investigation is left out of the scope of the thesis, but the graphs and insights are included in the appendix F.

It can be concluded that, by itself, the model cannot be validated and a comparison with the real-world behaviour of the prototype is vital to formulating any valuable claims about the model. To enable the comparison between the behaviour of the simulation model and the prototype, the simulation model is written to be fully parametric, see appendix C.1. This way, when the prototype is built and ready to be tested, the simulation model can be easily adjusted to

simulate the actual realised prototype. This enables the final validation of the model by simulating real-world interaction with the prototype by comparing them.

4 PROTOTYPE DESIGN AND IMPLEMENTATION

In order to be able to address the research goal, a force-feedback device was designed and built which adopts this novel hybrid drivetrain. This prototype is controlled by a custom electrical circuit and code and is capable of running 3 modes of force-feedback; fully passive, fully active or the novel hybrid mode. This enables assessment and comparison between each method whilst maintaining a constant framework.

This section divided into two parts; *Hardware and Manufacturing*, which addresses the design and physical realisation of the prototype; and *Software and Control*, which addresses the software and control-architecture used to realise proper force-feedback.

4.1 Hardware & Manufacturing

The prototype is based off of a educational force-feedback device called the HapKit from Stanford [17]. The HapKit 3.0 is simple and for the most part consists of 3d printable parts, see fig 13.

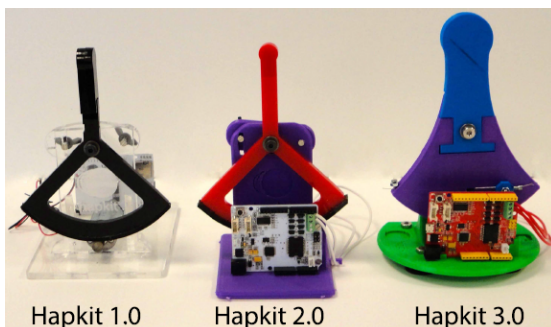


Fig. (13) Three versions of the Hapkit 1.0. Version 3.0 was designed in 2015 and exchanged the friction drive and laser cut structure for a capstan drive and a 3D printed structure. [18]

4.1.1 Design Elements

The prototype presented by this thesis, see fig 14 and 15, adopted the base design of the reverse pendulum end-effector and the capstan transmission, similar to the capstan transmission used by Baser in his 7 DOF haptic device [19], however, incorporates more electronics and two actuators; a brake and a DC motor.

The prototype has been designed completely with Solid-Works and any structural part is made of 3D printed PLA, which keeps the price of this prototype low and manufacturability high. In figures 14-18 on the next page all 3D printed components are modelled as light blue. Additionally, to aid in rapid prototyping and the possibility of easily interchanging parts, most of the assembly is kept modular, as such, many of the components can easily be changed,

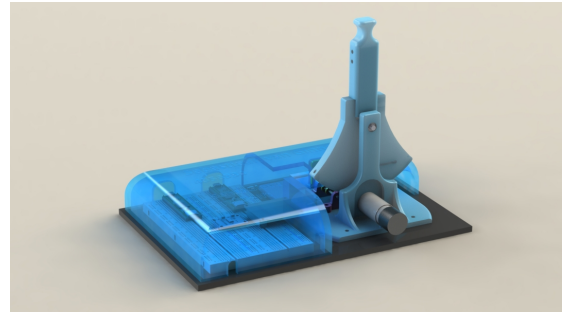


Fig. (14) 3D model render of the prototype, including electrical components and housing

adapted, or removed altogether. In the supplied figures (14-18 on the next page all bolts are left out for increased clarity. The empty holes shown are locations for these bolts.

As for the design, three ball bearings were used to reduce friction at the rotational shafts. The first bears the shaft about which the end effector and capstan wheel rotate, see fig 15. The other two, see fig 16 on the next page, bear the drive shaft which is connected to the DC motor and braking disc, see fig 17 on the following page.

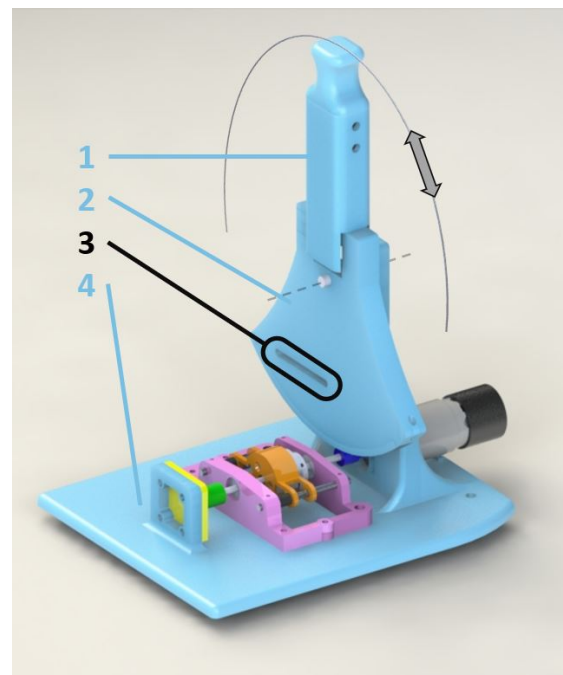


Fig. (15) 3D model render of the prototype, isolated to view mechanical components only.

(1) End effector encapsulating a loadcell; (2) Capstan wheel; (3) Tension slider for capstan; (4) Base of device

The electromagnetic brake consists of an electromagnet and a flat steel disc, fig 17 on the next page. Conventionally, this disc is pulled towards the electromagnet when a current is applied, making contact and generating a high friction force. This assembly, however, shifts the displacement responsibility to the electromagnet rather than the disc; the disc (point 4 in fig 17 on the following page is mounted on the shaft and, as such, cannot move from left to right. Therefore, the electromagnet has to move. This is done by creating a brake holder which holds the magnet and is

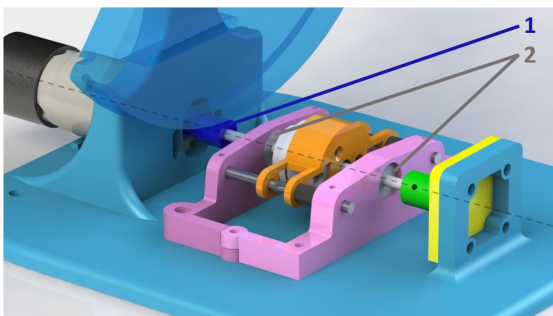


Fig. (16) 3D model render of the prototype, zoomed in on the brake assembly including the driveshaft.
 (1) Shaft Coupler and Capstan; (2) Bearing locations

capable of sliding over the two slider shafts, see fig 17. In order for the brake holder to detach from the steel disc whenever the current is shut off, the right sides of these slider shafts are spring loaded (between the pink brackets and the orange brake holder).

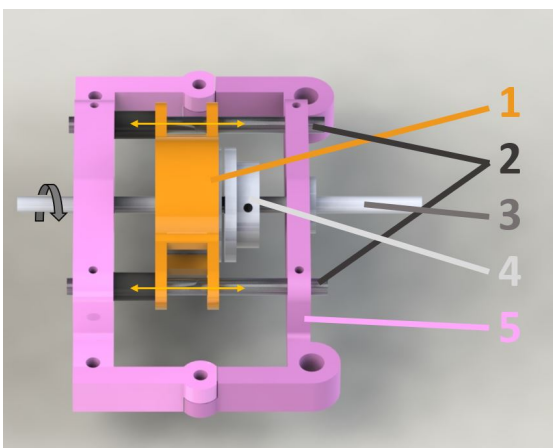


Fig. (17) 3D model render of the brake assembly, isolated to view mechanical components only.
 (1) Brake holder; (2) Slider shafts for (1); (3) Drive shaft connected to brake and DC motor; (4) Steel disc; (5) Modular brake assembly brackets

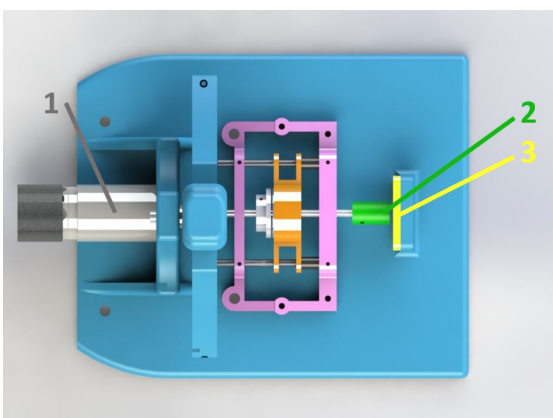


Fig. (18) Top view 3D model render of the prototype.
 (1) Faulhaber DC motor; (2) Magnet holder; (3) Holder for hall sensor

Furthermore, the prototype is capable of tracking its end

effector rotational displacement via a hall sensor, which works together with a dipole magnet at the end of the drive shaft, see fig 18. In addition, a loadcell integrated in the end effector captures the force exerted on the user's finger.

The prototype, as seen in fig 15 on the previous page is mounted on an acrylic plate together with the electrical components, which are in turn shielded by a fully 3D printed cover made of PLA, fig 14 on the preceding page.

4.1.2 Electrical Components

The prototype is powered by a lab power supply capable of 31 V. However, due to the motor controller being restricted to 16 V a maximum power supply of 16 V is used. This lab supply powers both actuators, the Faulhaber 2342S048C and the SenseGlove proprietary electromagnetic brake, via a MDD3A motor driver from Cryton. At 16 V the motor puts out about 4.16 N of force at the end effector. The components used are gathered in table 4 and their locations are shown in fig 19.

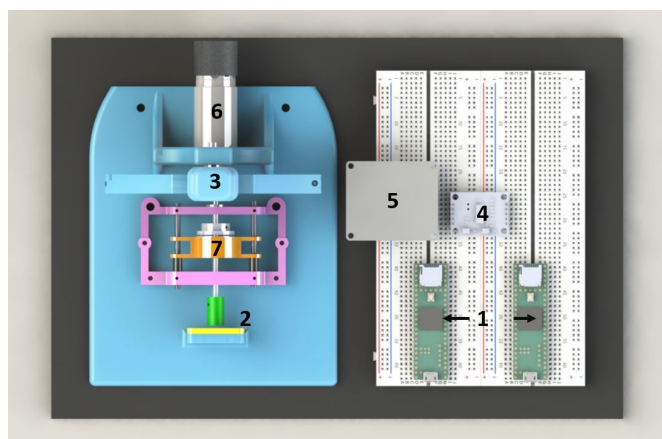


Fig. (19) Top view of 3D model render including electrical components, wiring is left out for clarity purposes, component names are gathered in table 4

4.2 Software & Control

In order to control the device and make sure the force output is as expected, the effective actuator characteristics have to be determined by measurement. This is due to unknown variables and deviations introduced by the transmission and other parts of the prototype which may impact the behaviour. The motor and brake force to voltage characteristics are found in the respective figures 22 on page 12 and 23 on page 12. Details about the retrieval of these figures can be found in appendix D. For control of the actual prototype, the linear R-curves are used to relate the power output of the actuator to the voltage input. Due to it being a first prototype, or proof of concept version, some errors are allowed as it should just prove the working principle. Optimisations and more complex relations can be incorporated in future versions.

The end effector's location must always be known for proper control and realistic force feedback. A hall sensor (AS5600) is utilised for this. A dipole magnet is attached to the end of the drive shaft within 1 mm of the hall sensor, this distance is required to capture adequate sensor data.

Component	Manufacturer	Function
(1) 2x Teensy 4.1	PJRC	Microcontrollers used for sending and receiving data between computer and hardware
(2) AS5600 hall sensor	SenseGlove proprietary	Position sensor used to collect positional data of the end effector
(3) Load Cell	Joy-It	Force sensor used to collect forces exerted on the end effector
(4) HX711 amplifier	Sparkfun	Force sensor amplifier used to amplify the load cell signal and convert it to usable data
(5) MD33A motor driver	Cryton	Motor driver used to drive the motor and the brake simultaneously
(6) 2342S048C DC motor	Faulhaber	DC motor used to drive the main shaft/end effector
(7) Electromagnetic brake	SenseGlove proprietary	Electromagnetic brake used to resist the main shaft/end effector
(8) 72-10480 Power Supply 0-30V	Tenma	Power supply for the motor driver and actuators

TABLE (4) Collection of electrical components used, details can be found in appendix C.2

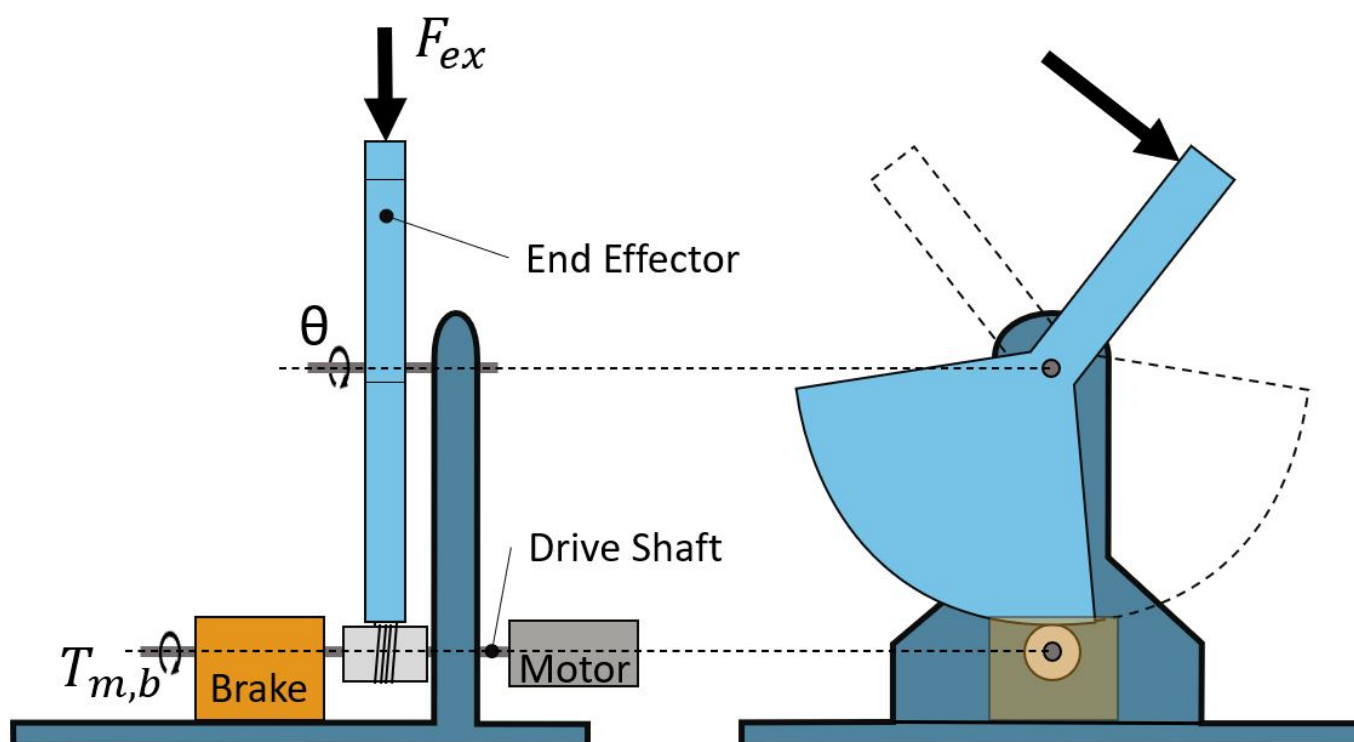


Fig. (20) Color coded schematic overview of the realised prototype, front and side view

This sensor tracks the rotation of the drive shaft in 12 bits, resulting in a drive shaft angle resolution of 11 counts per degree, which is sufficient to reliably track the position. The relationship between the end effector's rotation and the driving shaft must be established in order to determine the end effector's location. Since a capstan transmission is used to connect the two, this is done by simply dividing the radius of the connector on the drive shaft by the radius of the capstan wheel; 11 mm/75 mm. Due to the difference in radius, almost a factor 7, the drive shaft makes 1.7 revolutions when moving the end effector between its extreme positions; an angular rotation of 90 deg. The sensor does not track these revolutions. Instead, resets every time the drive shaft makes a full revolution; 360 \rightarrow 361 deg instead of 360 \Rightarrow 361 deg, which is needed in order to track the correct end effector position. As such an algorithm is devised in order to accompany for the drive shaft revolutions and correctly track the end effector position. This algorithm is included in the main code as in appendix C.1

Knowing the relation between input voltage and output force as well as the location of the end effector, the next step is to create the control of the system so the proper

voltage is sent to the actuators at the proper time, according to the simulation or task at hand. Two Teensy 4.1 microcontrollers are used to gather sensor data and send actuator commands. They are connected to a computer, which communicates with these microcontrollers via Python. The computer receives the sensor data from the microcontrollers and the Python script calculates the proper actuator command, which depends on the simulation or task at hand, and sends this back to the microcontrollers, which in turn translate this command into a voltage, which is then sent to the actuators, which generate the feedback force in the end effector. See appendix E for the full schematic of sensor data flow to feedback force and back again. One Teensy communicates with Python via a standard PyFirmata [20] protocol (StandardFirmata) which runs in the Arduino IDE and is included in the IDE when PyFirmata is installed. The other Teensy runs code based on a HX711 library from SparkFun [21]. This code is supplied in appendix ??

The Python model driving the prototype is designed to be fully parametric so as to facilitate rapid switching and altering of the virtual environments and actuation methods. However, this prototype is limited to environments or

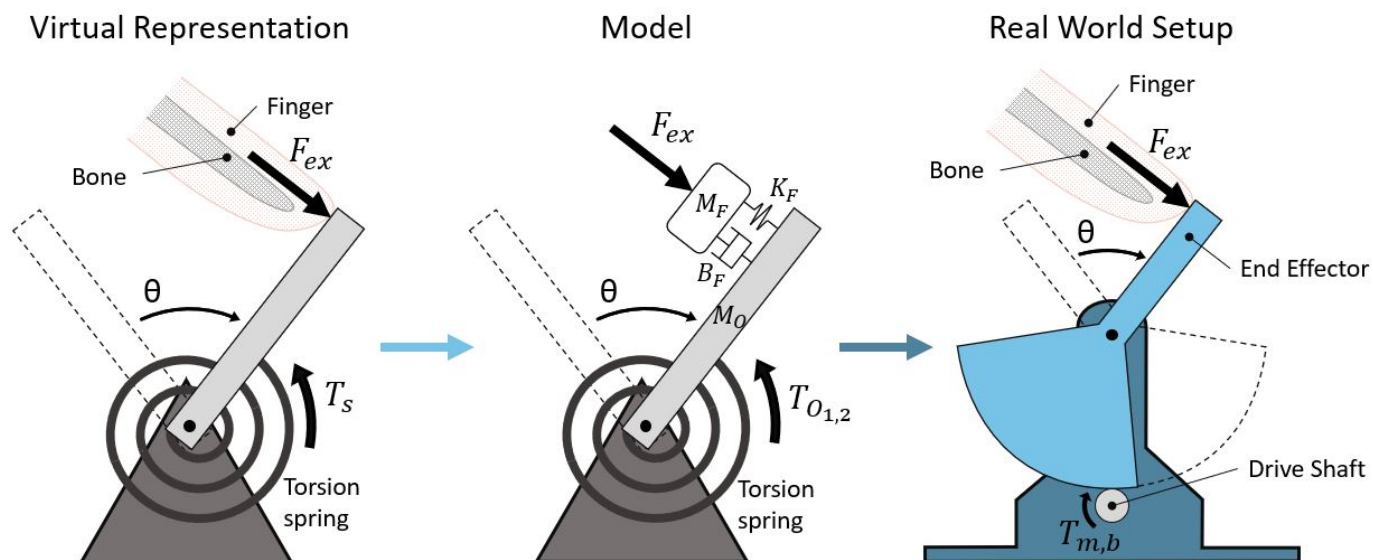


Fig. (21) Three figures indicate the translations between the virtual object; a torsion spring connected to a beam (left), the model used to represent this virtual object (middle) and the realised prototype (left) used to generate the appropriate force feedback

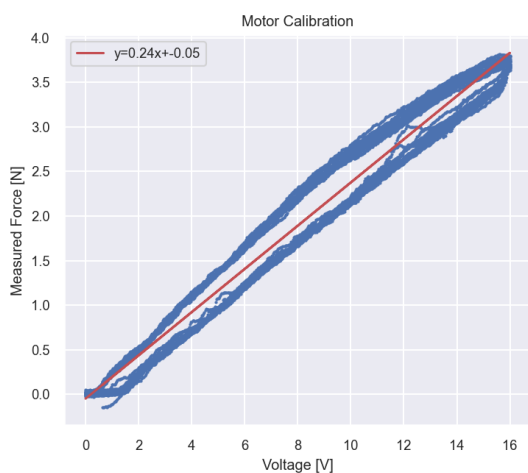


Fig. (22) Graph showing the relation of input voltage to input output force of the used DC motor

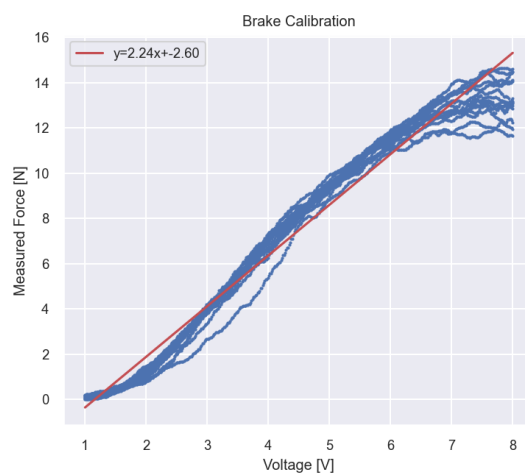


Fig. (23) Graph showing the relation of output force to input voltage of the used electromagnetic brake

objects consisting of one degree of freedom but could be altered with relative ease to accompany for more advanced and complex environments in the future. The system is completely closed loop which means that the measured user input force at the end effector is used as input force in the model in addition to the location and velocity of the end effector. This enhances the usability of the device greatly and makes the switching between actuation modules (motor and brake) more predictable and fluid. The discussion elaborates further on the differences between using the prototype open-loop and closed-loop.

4.3 Simulation to Prototype comparison

Figure 24 on the following page compares the actuator force output and states of the simulation model to those

of the prototype upon user interaction. A simple forward-backward motion on the end effector is introduced by the user, and this force, F_{ex} , is captured along with the state parameters θ and $\dot{\theta}$. The model is then fed with this captured user input force, F_{ex} , in order to replicate the real interaction with the prototype. The output is then calculated in terms of actuator voltage, displacement, and angular velocity. In the figure, Feedback Force Simu refers to forces $F_{O_{1,2}}$, External Force refers to the measured user force F_{ex} and lastly, Feedback Force Real is the force generated by the actuators. This force is directly proportional to the voltage sent to the actuators, as explained in 4.2 on page 10, which in turn is dictated by the displacement, θ , as the virtual object is a spring; $F = -k * u$.

The results, shown in 24 on the following page, clearly indicate that both in reality and in the simulation, the oscillatory behaviour which was previously found did not

Reality vs Simulation - Behaviour in Time

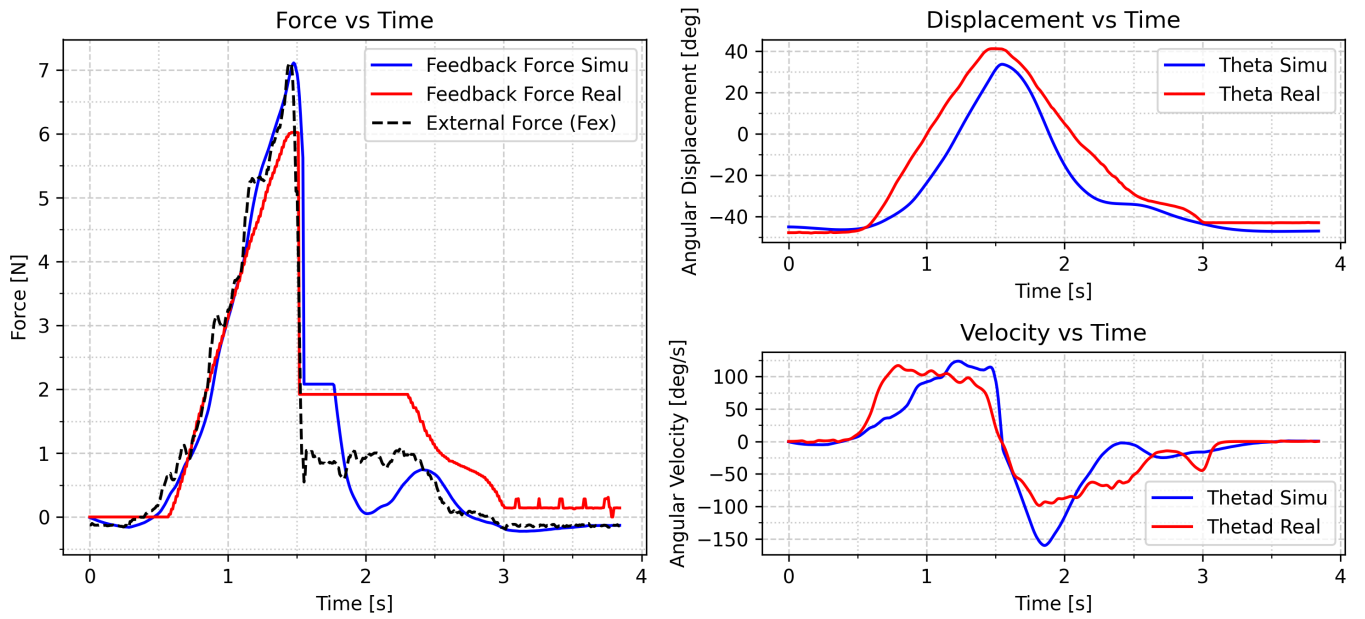


Fig. (24) This figure is a collection of 3 plots with time on the x-axis. The y-axes of the plots indicate the force and states of the prototype interaction (real) and the simulation (simu). "External Force" is the input force of the user exerted on the end effector, which is captured and fed into the simulation as F_{ex} . The object parameters chosen for the environment were; $K_O = 4$, $B_O = 1$ and $M_O = 0.1$. These last two values were chosen by trial and error to make the simulation plots resemble the "real" plots as much as possible. This is by no means the optimal setup, and due to time constraints, no study was conducted to further optimise it

occur for this particular test. Looking at the profile of F_{ex} , it can be observed that there is a significant reduction in all forces when the motion direction switches. This is due to the switching of the actuator activity from brake to motor. As previously stated, this switch occurs whenever $\dot{\theta} = 0$. Unlike in the simulations, the recorded External Force drops together with these actuator forces; the user drops his/her input force until the end-effector starts pushing back the users' finger, which only happens when the user input force drops below the maximum force output of the motor (2.08 N). Due to this behavior, the oscillations do not occur. The reason the user drops his/her force drastically is mostly due to the narrative of the task objective; moving the end-effector back and forth. In the simulations, however, a sinusoidal curve is used as an input, which is rigidly fixed in time. The task objective used in the experiment is a more natural way of interacting with the prototype, and therefore it is a positive remark that the prototype, using hybrid force feedback, behaves more reliably in such cases.

In some cases, which were executed in an exploratory manner, oscillations were observed. However, this was caused in part by limitations of the code, delays, or other unwanted artefacts rather than the nature of the drivetrain. However, due to time constraints, no investigation was performed into these anomalies. Other than that, oscillations were sometimes observed when modelling the spring + wall environment, more on this in the discussion.

Other than that, comparing the real and simulation states, θ and $\dot{\theta}$. The model, in the case of the linear spring environment, does quite a good job of reflecting reality.

The two curves for the angular displacement, θ , are similar in terms of reaching their maxima and minima at similar points in time. However, the slopes in between do differ slightly, which is reflected in the curves showing $\dot{\theta}$; the simulated angular velocity seems to vary more than the velocity in reality does and also increases at times when the real velocity is actually decreasing. However, the overall behaviour could be described as similar in terms of maxima, minima, and overall shape. The differences in the angular velocity could be explained by a damping coefficient or mass not reflecting reality, which, of course, has an impact on the system. As these values were retrieved by trial and error, it is logical to assume that they are not tweaked to perfection. This could be picked up as a research topic to explore in the future. Another reason could be that in the model, the actuator forces are related directly to the user input force; $F_{O_{1,2}} = F_{ex}$. However, in reality, the actuator forces are based on the location of the end effector, so in reality there is a discrepancy between the user input force and the actuator force, as their relationship is indirect.

5 PROTOTYPE VALIDATION

5.1 Mechanical Rendering Ability

In order to validate the prototype and assess whether practise confirms the benefits of the theory. The prototype needs to be evaluated both in a mechanical sense and a perception-based evaluation. In order to assess the benefits, the prototype should be compared to the state-of-the-art actuation types; active and passive. Capturing the capabilities and

limitations of the prototype, as well as their active and passive counterparts, enables proving or disproving the benefit claims presented in this thesis. To evaluate the mechanical performance of the hybrid prototype, a qualitative comparison is made between the force feedback rendering range of the 3 methods; hybrid, passive, and active. To establish such a comparison, the characteristics of the different modes need to be captured. This is established by using the Force to Voltage graphs (figs 22 on page 12 and 23 on page 12) together with the knowledge of how each mode uses each actuator. Due to the non-linearity of the hybrid method, a distinction is made between motion directions.

This method gives insight into the very basis of mechanical performance; a one-dimensional rendered force range. It is crucial to establish this knowledge in order to validate the prototype, as without knowledge of the force output range per actuation method, there is no way of assessing which method should outperform the others, and this expectation can then be accepted or rejected by a human-in-the-loop validation. Furthermore, it is a basis for shaping the potential of the hybrid actuation method, creating focus for future research. Of course, this comparison is limited by the prototypes' physical capabilities and hardware components, but by using the same device and the same components, and only changing which actuators are active, the comparison is still valid.

During forward motion, compressing the virtual object in this case, the maximum force of the brake, at 8 V, is over 13.5 N, see fig 23 on page 12. To be conservative, the maximum resistance force of the brake will be assumed to be 13 N. From fig 22, and previously stated, the maximum forces of the motor at 16 V and 8 V are 4.16 N and 2.08 N respectively.

Furthermore, the brake has a voltage threshold under which it generates no force. This is due to the air gap between the steel plate and the electromagnet, see fig 17. Through trial and error, this threshold was discovered to be approximately 1 V. Any forces or stiffnesses which demand a force between the given maxima or minimum can be generated by the actuators.

The above is visualised in fig 25, in which the blocked areas visualise the force generation ability of each operation mode; passive, active, and hybrid.

5.2 Human-in-the-loop Validation

The above evaluation technique addresses the mechanical capabilities. However, to validate the prototype, some user experience and perception evaluation has to be taken into account; the prototype can function mechanically superior, but might still not be able to render high quality haptics. As such, a user experiment is set up and the data is captured to compare the haptic quality of the hybrid operation mode to conventional modes. The results of the experiment are gathered in figures 28 on page 16 and 29 on page 17. A collection of all conducted trials is added in appendix G.

A simple human factors experiment is performed to gain a general overview and insight into the perceived physical fidelity of the prototype. Therefore, assessing what is proposed by the results of the mechanical evaluation and therefore checking whether the human perception also

reflects the proposed advantages or disadvantages of using hybrid force feedback.

5.2.1 Subjects

A haptic feedback experiment is conducted to compare the performance of the hybrid operation mode to fully active or fully passive operation. Due to the exploratory nature of the experiment and time constraints, it is conducted by just one participant.

5.2.2 Task

The task consists of testing the three modes in two environments; one which simulates a spring (a linear stiffness) and one which simulates this same spring but now there is also a virtual wall which is located inside the virtual environment. The previously mentioned figures 26 on the following page and 27 on the next page show the two environments in a 2D fashion, with the device pictured along with the virtual environment components (spring and wall). Both of these environments have only one degree of freedom. The angular displacement, θ , is linearly related to the spring, and the actuator voltage is set to maximum at the location of the wall (16 V for the motor and 8 V for the brake). The feedback force is depicted in the figures as torques; $T_{O_{1,2}}$.

In total, there are 6 different tests. For each test, the environment is known to the participant but the actuation mode is not. A fully blind setup is not necessary as the aim of the experiment is to see how each mode well renders a specific environment based on the participants' perception. As such, knowing which environment is being rendered is vital. To ensure the participant cannot gather information from the surroundings regarding which actuation mode is active, the user is wearing headphones playing white noise and the actuators are visually covered. Also, before executing the task, the participant is given time to familiarise with the device without any actuation being activated.

To gather richer and more reliable results, every setup (mode + environment) is performed six times, resulting in a total of 36 tests the participant executes. For each test, the participant is asked to move the end effector forward and backward once, whilst trying to keep a similar velocity in every test, so as to ensure better comparability between the tests. Also, the participant is instructed to keep the end effector in the device work space (-45 deg to 45 deg); pushing against the end effector when it cannot move further, the extreme positions, will give false force data as it is a physical limitation of the prototype and not part of the virtual environment. Lastly, each test takes no longer than 4 seconds, with a pause of at least 5 seconds between each test.

5.2.3 Analysis

On a 5-point Likert scale, the participants' perceptions are compared to their expectations after each test. In addition, experiment data is captured, reviewed, and gathered into concise graphs indicating the significant performance differences between the modes of actuation in each environment. These results identify the added value of using the hybrid operation mode compared to the conventional modes. This is further discussed in 6.

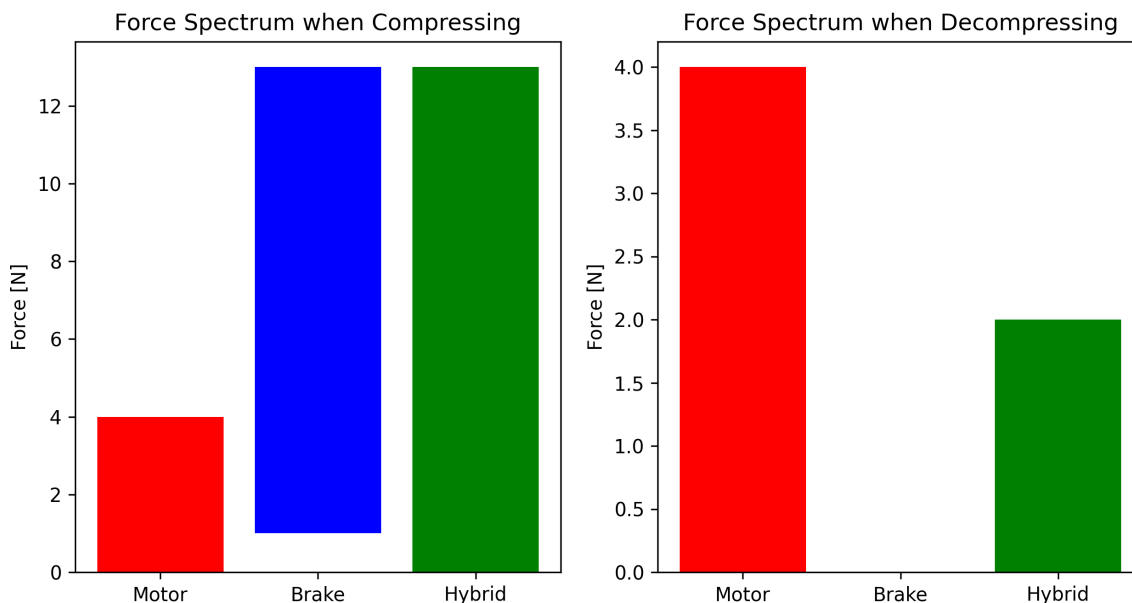


Fig. (25) Visualization of the forces which are generated by each actuation method, differentiated between compression and decompression, as these differ for the brake and hybrid actuation mechanisms. These values are valid for any position of the prototype end effector

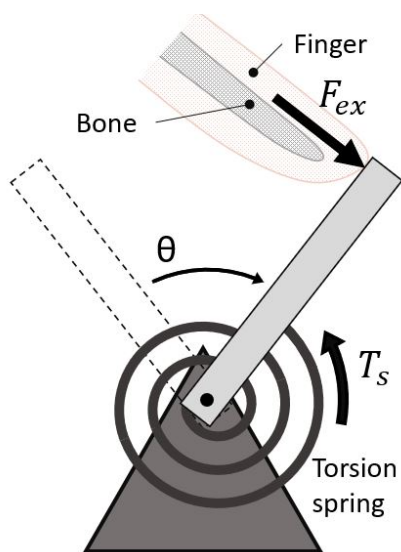


Fig. (26) Representation of the virtual environment consisting of a virtual compression spring

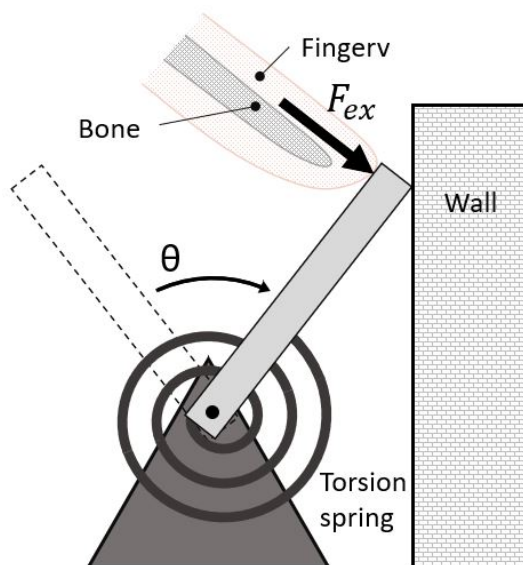


Fig. (27) Representation of the virtual environment consisting of a virtual compression spring and a virtual wall

5.3 Experiment Results

5.3.1 Spring Environment

5.3.1.1 Active: In fig 28 on the following page, the average of the results for each actuation method is captured when performing the spring environment test. As expected, the active actuation method is perfectly capable of rendering the virtual spring, as long as the DC motor is capable of delivering an adequate magnitude of force, a maximum of approximately 4 N. As such, the motor cannot adequately render the stiffness above 4 N and the force line in both the force vs time and force vs displacement plots flattens

out until the motion is reversed. Looking at the force vs displacement plot, a force discrepancy between the forward and backward motion is visible; the line is not a single linear diagonal line, which is normally associated with a force vs displacement plot of a linear spring. However, the captured force is not the force exerted by the spring, but rather the force applied by the user. This force is not equal to that of the virtual spring or actuator output; in order to move forward, the user input force has to be higher than the actuator force output and vice versa, creating the force

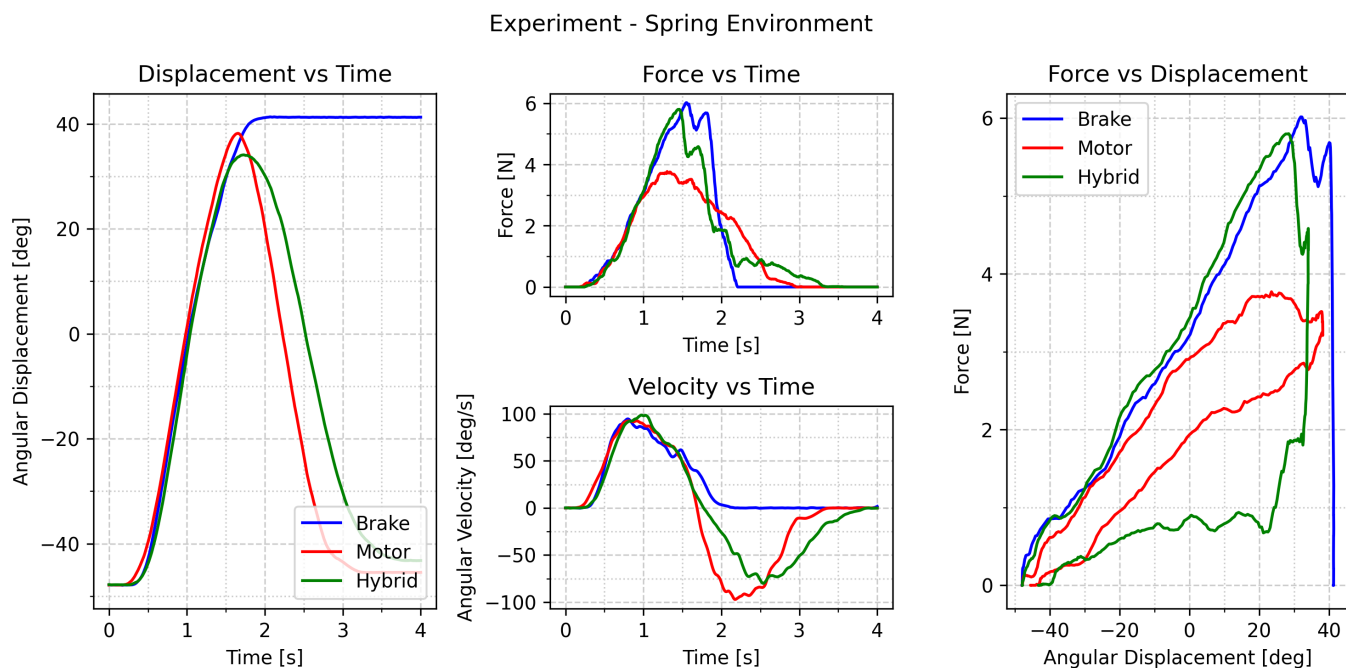


Fig. (28) Shown, is a visual representation of the experiment results. Each line represents the average of the 6 test runs conducted with each actuation method. Three plots are plotted against time; displacement, force, and angular velocity. The plot to the far right is a force vs. displacement plot. These plots give insight into how each actuation method behaves within the tested virtual environment and show how they differ

discrepancy visualised in the force vs displacement plot. Furthermore, the displacement and angular velocity plots appear as expected; the forward and backward motions are captured well and the lines are smooth.

5.3.1.2 *Passive*: The passive method, brake only, is capable of adequately rendering the virtual spring during its forward motion. Velocity is quite stable, displacement rises smoothly, and the force curve covers the required force spectrum of this particular stiffness. However, it is incapable of rendering the linear stiffness along the full pathway; end-effector forward and backward again. Since the brake can only generate a resistive force when the user reduces its force input and ultimately breaks away from the device with its finger. The end-effector remains in the same state, so during the backward motion there is no feedback force and no velocity. This is illustrated in the graph on the left of the figure, displacement vs time at approximately 1.8 s. The displacement does not change, even though the user input force eventually reduces to zero (see force vs. time plot). This is also apparent in the force to displacement graph. The forward motion is captured by the sloped curve which stops at about an angle of 40 deg. This is where the user starts to exert less force in order to change the direction of motion. As expected, there is no trace of the backward motion; there is no displacement and no force captured.

5.3.1.3 *Hybrid*: Lastly, the displacement vs time curve of the hybrid feedback is almost identical to the respective motor curve. indicates that the behaviour during the experiment averaged over 6 trials is very similar. This is remarkable as the force discrepancy upon motion inversion is significantly larger, as seen in the force vs displacement graph, at 32 deg as well as the force to time graph, at

approximately 2 s. This discrepancy is explained by the fact that during the backward motion, or decompression of the spring, the weaker motor takes over force generation.

Furthermore, the graph shows nothing notable about the behaviour of the hybrid actuation method other than that it seems to perform as well as the active, DC motor, method, looking at the state plots; displacement and velocity vs time. The only difference being that for the hybrid approach, the backward motion is a little more stretched and the motion reversal happens slightly earlier, which can more likely be attributed to a slight deviation in user control than a mechanical deviation.

5.3.2 Spring + Wall Environment

The results of the tests involving the environment including the wall, are shown in fig 29 on the next page. The wall has been positioned at 26.6 deg. Other than that, all parameters are exactly as in the spring environment. As the end-effector reaches the angular displacement of 26.6 deg the actuators are sent maximum system voltage (8 V for the brake and hybrid methods (16 V for the active method), thereby generating maximum force, which in turn should render the effect of pushing against a rigid wall.

5.3.2.1 *Active*: The force vs displacement and force vs time graphs clearly show displacement past the location of the wall, which indicates that the active actuation method, using this DC motor, is not capable of rendering the wall as a rigid object when powered by 16 V, in fact it maxes out on the expected 4.16 N. However, even if the generated force were sufficiently high to fully stop the users' input, still, the interaction would never truly feel like a wall or a rigid object. Due to the dynamics of a DC motor and

Experiment - Spring + Wall Environment

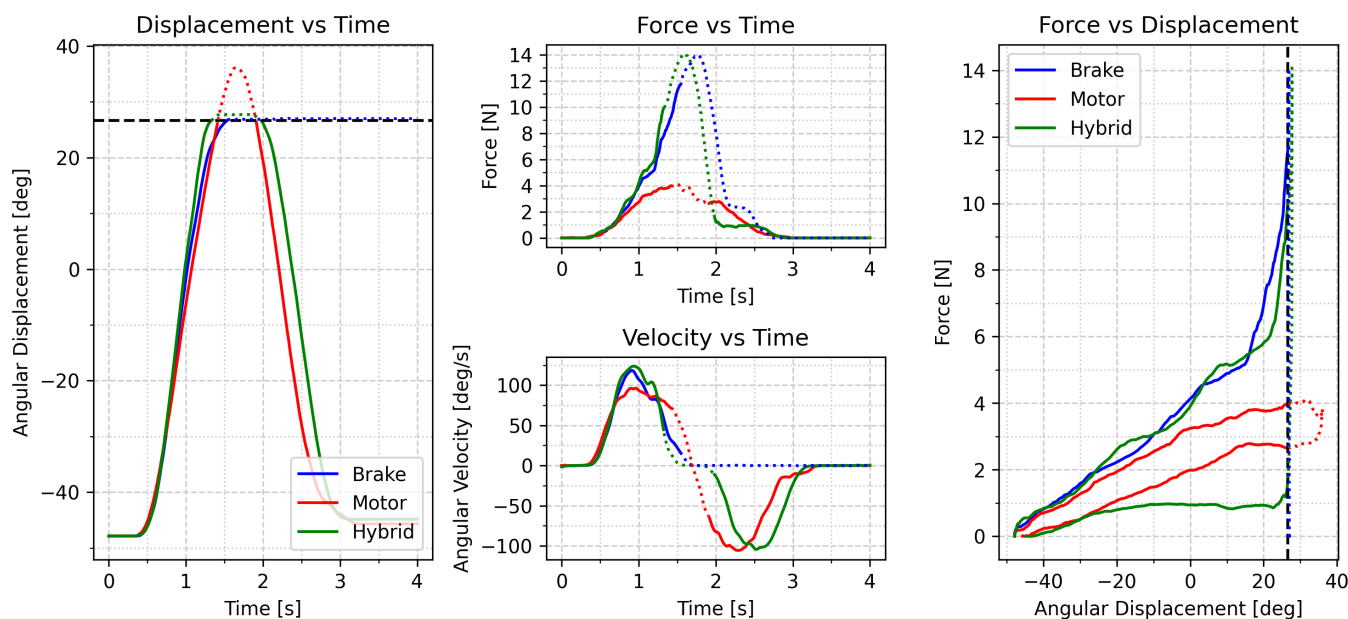


Fig. (29) Shown, is a visual representation of the experiment results. Each line represents the average of the 6 test runs conducted with each actuation method. Three plots are plotted against time; displacement, force, and angular velocity. The plot to the far right is a force vs. displacement plot. These plots give insight into how each actuation method behaves within the tested virtual environment and show how they differ. The dotted parts of the lines indicate whenever the end effector is on or past the location of the virtual wall. In an ideal world, the user should not be able to move past the virtual wall

the nature of active force feedback, hitting a wall is an instantaneous process, whilst a motor will always need to spool up, which would create some kind of damping effect. The other graphs indicate the same shortcoming, angular velocity never settles at zero during the wall interaction. All plots look very similar to those without the added wall, which is quite logical as all other parameters in the environment are the same.

5.3.2.2 Passive: The passive method, only brake, indicates the same problem as during the previous test. The backward motion is not captured and the state of the end-effector remains the same upon lowering the user input force. However, the wall is rendered as expected; whenever the end effector reaches 26.6 deg, the angular velocity drops to zero and the force starts to rise. The exerted force never exceeds the force of the brake, and as such, the velocity remains at zero; displacement remains unchanged. As such, the brake is capable of rendering the forward motion part of the interaction with this environment, but fails when moving backwards (decompressing the virtual spring).

5.3.2.3 Hybrid: Again, the hybrid feedback method seems to render the virtual environment in a proper fashion. This is best illustrated in the displacement to time graph; as the end effector reaches the location of the wall, the displacement remains constant, up until the user drops his/her input force and the end effector starts to move back again due to the pressure of the virtual spring. The interaction with the wall, indicated in the force to time plot, is, logically, very similar to that of the brake. As the wall is reached, the velocity drops to zero and the force starts rising.

This wall interaction is also clearly illustrated in the force vs displacement graph. It is only when the users' input force drops below approximately 2 N, that the backward motion starts, velocity goes to negative, and the end effector eventually ends up in its original state, just like what happens during the active method. Both the displacement and velocity curves look smooth and as such there is nothing to note. Again, the state vs time plots of the hybrid method look a little stretched out during the backwards motion compared to the active method, for similar reasons as explained before. In the displacement vs time graph, it can be noticed that the angular displacement seems to extend past the location of the wall. The reason for this deviation is unclear and could be investigated in future research.

5.3.3 Experiment Results Summary

To summarise, purely by looking at the data and graphs at hand, it can be deduced that the passive actuation method is incapable of correctly rendering any of the two environments. The active method was capable of rendering the stiffness correctly to some extent, until it flattened out at its maximum force output. However, it proved incapable of rendering the wall in the spring + wall environment, for similar reasons; a limited maximum force output. Lastly, the hybrid approach proved to be capable of rendering both environments without showing unwanted behaviour such as oscillations or other unintended mechanical dynamics due to the hybrid setup.

This would lead to the suggestion that in these particular cases, the hybrid setup would be the most optimal one.

However, the users' perception should also be taken into account to assess the achieved physical fidelity, which is of paramount importance to achieving high quality haptics.

5.4 Survey, 5-point Likert scale

To further validate the hybrid drivetrain and its haptic quality as built in the prototype, information regarding the user perception is gathered. Following each test, the participant is asked to respond to a question on a 5-point Likert scale, with responses ranging from strongly disagree to strongly agree. The questions asked after the tests were, respectively, for the spring and spring + wall environment:

- During this test I clearly felt forces I would associate with interacting with a linear stiffness?
- During this test I clearly felt forces I would associate with interacting with an infinitely rigid object, such as a wall, in addition to a linear stiffness?

The results of the questions are shown in fig 30 on the following page. It is clearly observed that both the active and passive methods do not do a great job of generating the perception of a spring like interaction in conjunction with being able to render an infinitely rigid object, in this case a wall. Furthermore, the active method does perform best in the Spring environment. Better than the hybrid setup, despite the earlier mentioned graphs indicate similar performance, this limited perception survey indicates differently. This is probably due to the different actuators at work when moving forward or backward during hybrid actuation. However, still seems to convey the correct senses. The brake also fails perception wise when trying to render the spring environment, this is expected as there is no force feedback when moving your hand backwards; the end effector stays in place. Overall, the perception survey indicates a similar result as the data analysis of the experiment; the hybrid actuation method is capable of rendering and conveying the idea of interaction with both environments, whilst passive and active cannot. This does not mean that the hybrid feedback approach is the ideal solution in all cases, but in this particular case, with these particular parameters and environments, it is the favored actuation method.

6 DISCUSSION

6.1 Simulation Model

The simulation model seems to be very dependent on the data. When given force data from the prototype, the model behaves in a way that is mostly true to life. The model may not give correct results when fed data that was not acquired using the prototype, so it is necessary to evaluate the plausibility of each input before evaluating the model's output. Due to the aforementioned, the model isn't very useful for exploring how hybrid drivetrain force feedback could be used without a prototype. Due to time constraints, the model's dynamics were simplified and some parameters were chosen by trial and error. To make the model a more useful tool, additional research must be undertaken, and model parameters must be added or modified to reflect reality and be able to handle more nuanced and complex

situations. Future research should also address the implementation of suitable delays and signal processing in order to more properly simulate real actuators and real interactions, which are never instantaneous.

6.2 Prototype

6.2.1 Mechanical Ability

The hybrid drivetrain, as implemented, is capable of rendering the tested environments, which cannot be claimed for active and passive approaches. However, the hybrid approach does suffer from some major flaws. During exploratory testing, it was determined that the prototype's behaviour while interacting with walls was inconsistent. On occasion, the brake would disengage and the user would be able to proceed past the wall, which is undesirable.

Whenever the end effector reaches the location of the wall, the brake is fully engaged and the velocity lowers to zero. Due to the velocity lowering to zero and the control rule mandating the release of the brake and starting of the motor, this would generate the oscillating behaviour observed in simulations if the user does not reduce his/her force input considerably before the brake disengages.

This was remedied by measuring the force exerted by the user and incorporating that information back into the control sequence, creating a closed loop. The brake now only disengages whenever the velocity is zero or negative and the user input force is lower than a certain force threshold. However, sometimes this would not trigger and the following would happen: the user overshoots and the brake engages again, recreating the theoretic oscillatory behaviour for a number of repetitions until the user force drops. Due to time restrictions, defects in the code, allowing for this undesired anomaly, were not resolved. It is a defect in the control system, not the mechanical dynamics of the drivetrain, and future research should investigate why this occurs.

Other than that, the hybrid approach properly and consistently joins together two conventional means of actuation; passive and active. It builds on the strength of both conventional methods whilst suffering from minimal negatives, as per the controlled and limited circumstances of this study. A big limitation of this study is that the influence of damping is taken out of the study as much as possible. The participant is asked to move the end effector with the same, and constant, velocity in every trial. This does make data comparable, but it gives very limited insight into how velocity, and therefore damping, influences the system. In order to fully understand the dynamics of the system, future research should include tests with different end effector velocities to understand the effects of damping.

The application in this study is quite specific, and future research should aim to broaden the tested and testable application spectrum to acquire a greater understanding of the exact strengths and drawbacks. It should be noted that the maximum force the motor could produce was limited in the prototype by the used motor driver, which had a limited voltage of 16 V. In future versions, a motor driver capable of 48 V could be used in order to power the DC motor to its full potential, or a version of the motor which delivers its maximum torque at a lower voltage could be

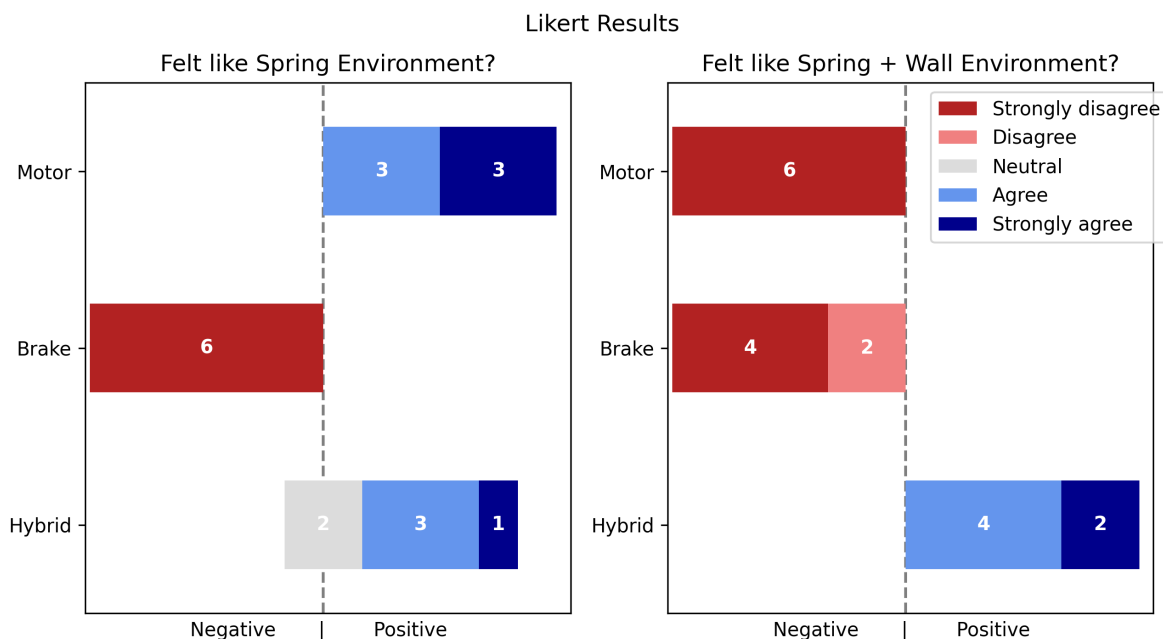


Fig. (30) Likert test results from both environments in 2 plots. The different actuation methods are shown on the y-axis. The x-axis differentiates between positive and negative responses; the colour of the boxes indicates the severity of the response. The number in the box is the number of particular responses

used. However, due to the motor force to voltage ratio being linear, the maximum force output of this motor would then be approximately 12N. which is still substantially lower than the brake and not enough to render the virtual wall. As such, the results would be similar.

Building on the argumentation favouring the hybrid drivetrain, potential weight benefits, as per appendix A, could be achieved when implemented properly. It should be considered that structural components used to house the actuators and transmit the forces are not taken into account in the weight calculation, but these should not deviate significantly from a completely active design.

Overall, it appears that the hybrid approach could be a mechanically advantageous addition to wearable haptics due to the variety and quality of the generated haptics as well as the potential weight advantage.

6.2.2 Perceptual Ability

Perceived physical fidelity is a crucial component in haptics. Even if a haptic device appears to perform flawlessly and data seems to enforce this statement, it may still be disqualified if the user perception is inadequate or if the device is extremely uncomfortable to use. A survey was conducted in order to assess the perceived quality of the haptics. The results of the perception survey are favourable towards hybrid feedback in the specific circumstances evaluated, bolstering the rationale for future research into hybrid force feedback drivetrains and their implementation in the wearable force feedback industry. However, due to time limits, just one participant was included in the survey that was completed. As a result, no significant conclusions can be derived from the survey data, which serves merely a suggestive function.

6.3 Reflection on Literature

In the context of the wearable force feedback spectrum, the prototype could ultimately be embedded in a wearable and wireless system like the SenseGlove Nova [4] at the cost of some weight. As the brake present in the Nova is used in the prototype, adding a small motor to achieve the active part of the feedback would already result in a proper hybrid drivetrain like suggested by the prototype. With the addition of this active feedback, the device would be able to render a vastly wider array of interactions, mostly involving stiffness, than passive wearables like the Wolverine [8] or the SenseGlove Nova. All the while being potentially lighter and stronger than active wearables like the CyberGrasp [12] or the SAFE glove [10] due to the passive actuator addition.

The prototype uses the motor at 1/6th of the maximum voltage (48 V), meaning the motor in the prototype puts out 1/6th of its maximum power. Together with the knowledge in appendix A, it can be deduced that the motor could be made 6x smaller and lighter and still put out a similar force. Even though the motor cannot be directly scaled down and many nuances are at play, this is a rough indication of what is possible at these magnitudes of force. The combined weight of this scaled down motor and the SenseGlove brake would be 42 grams. This means that interchanging the brakes with these hybrid components would only add to the glove, bringing the total weight to 380 grams, which is similar to the state of the art Exoten glove [22] whilst being completely wearable, wireless, and provide haptics to 4 fingers individually.

The device fits right in the gap which the state of the art leaves untouched. Enabling a higher physical fidelity in wireless and wearable haptic solutions, opening up new possibilities and widening the application potential of these

devices. Due to the relative simplicity of the design, the drivetrain could easily be scaled up and down in order to be applied in a wider range of sectors where this hybrid drivetrain technique would be of added value. SenseGlove, the client, is positive about the prototype as well and intends to build further on the design in order to finally implement into their products.

7 CONCLUSIONS

The use of a hybrid drivetrain, by coupling a motor and a brake, is proposed. By strategically engaging each actuator for tasks at which they typically excel, high quality haptics can be established whilst potentially reducing the total actuator weight. First a theoretical analysis into the proposed drivetrain is conducted after which this actuation method is compared to an active and a passive actuation method during an experiment where the participant is asked to interact with two different environments using all three methods after which he/she is asked to fill in a survey regarding the perceived physical fidelity.

The theoretical analysis showed promising results regarding the use of the hybrid drivetrain, however some undesired behaviour was found. This behaviour is explained by the inputs being prescribed, it is hypothesized that this will not be as pronounced when interacting with the prototype due to a human being able to adapt to the situation. From theory and enforced by the theoretical analysis, the hybrid method should outperform the active and passive systems as those both have their clear drawbacks; passive cannot render a low stiffness whilst the active motor cannot render a rigid wall, whereas the hybrid method should be able to render both. The experiment enforces this theory and indicates a clear mechanical advantage over the state of the art. The results of the survey further enforced this mechanical advantage by indicating that the hybrid drivetrain can give the sense of interacting with both tested environments, however this serves merely as a suggestion due to only one participant being surveyed.

This thesis brings forward that using a hybrid drivetrain, within the constraints of the research, has its clear advantages over the state of the art. However, also introduces a challenge; the force discrepancy between the active and passive elements can introduce unpredictable behaviour. In order to acquire a deeper understanding of the working principle, future research should focus on improving and expanding the control- and simulation-model. The control model, in order to more precisely reflect the virtual object and to account for the physical limitations of the device. The simulation model to be able to do exploratory research without the need of a physical device. Many nuances, like friction and gravity, are still left out for simplicity purposes, however should be investigated on their influence on the system. Lastly, research should be done into incorporating a smaller, more representative motor in order to investigate the possibilities of down scaling the prototype.

ACKNOWLEDGMENTS

I am very grateful for the help of Prof. Dr David Abbink, Dr. Michaël Wiertlewski and Johannes Luijten, their knowledge and their helpful feedback. Thanks to SenseGlove for supplying me with the materials, tools and space to create and test the prototype.

REFERENCES

- [1] F. Mantovani, G. Castelnuovo, A. Gaggioli, and G. Riva, "Virtual reality training for health-care professionals," *CyberPsychology & Behavior*, vol. 6, no. 4, pp. 389–395, 2003.
- [2] A. Lele, "Virtual reality and its military utility," *Journal of Ambient Intelligence and Humanized Computing*, vol. 4, no. 1, pp. 17–26, 2013.
- [3] J. I. Lipton, A. J. Fay, and D. Rus, "Baxter's homunculus: Virtual reality spaces for teleoperation in manufacturing," *IEEE Robotics and Automation Letters*, vol. 3, no. 1, pp. 179–186, 2017.
- [4] "SenseGlove Nova," 2021. [Online]. Available: <https://www.senseglove.com/product/nova/>
- [5] "Da Vinci Systems," 2021. [Online]. Available: <https://www.intuitive.com/en-us/products-and-services/da-vinci/systems#>
- [6] M. Sierotowicz, B. Weber, R. Belder, K. Bussmann, H. Singh, and M. Panzirsch, "Investigating the influence of haptic feedback in rover navigation with communication delay," in *International Conference on Human Haptic Sensing and Touch Enabled Computer Applications*. Springer, 2020, pp. 527–535.
- [7] M. Bouzit, G. Popescu, G. Burdea, and R. Boian, "The rutgers master ii-nd force feedback glove," in *Proceedings 10th Symposium on Haptic Interfaces for Virtual Environment and Teleoperator Systems. HAPTICS 2002*. IEEE, 2002, pp. 145–152.
- [8] I. Choi and S. Follmer, "Wolverine: A wearable haptic interface for grasping in vr." Association for Computing Machinery, Inc, 10 2016, pp. 117–119.
- [9] J. M. Ochoa, Y. Jia, N. Dev, and D. G. Kamper, "Development of a portable actuated orthotic glove to facilitate gross extension of the digits for therapeutic training after stroke." *IEEE Computer Society*, 2009, pp. 6918–6921.
- [10] P. Ben-Tzvi and Z. Ma, "Sensing and force-feedback exoskeleton (safe) robotic glove," *IEEE Transactions on Neural Systems and Rehabilitation Engineering*, vol. 23, no. 6, pp. 992–1002, 2014.
- [11] I. Sarakoglou, A. Brygo, D. Mazzanti, N. G. Hernandez, D. G. Caldwell, and N. G. Tsagarakis, "Hexotrac: A highly under-actuated hand exoskeleton for finger tracking and force feedback." vol. 2016-November. Institute of Electrical and Electronics Engineers Inc., 11 2016, pp. 1033–1040.
- [12] "CyberGrasp," 2022. [Online]. Available: <http://www.cyberglovesystems.com/cybergasp>
- [13] D. Wang, M. Song, A. Naqash, Y. Zheng, W. Xu, and Y. Zhang, "Toward whole-hand kinesthetic feedback: A survey of force feedback gloves," *IEEE Transactions on Haptics*, vol. 12, pp. 189–204, 4 2019.
- [14] "Haptic workstation," 2017. [Online]. Available: <http://www.cyberglovesystems.com/haptic-workstation>
- [15] "Serie," 2022. [Online]. Available: <https://www.faulhaber.com/nl/producten/serie/2342cr/>
- [16] Q. Bi, C. J. Yang, X. L. Deng, and J. C. Fan, "Human finger mechanical impedance modeling: Using multiplicative uncertain model," *Proceedings of the Institution of Mechanical Engineers, Part C: Journal of Mechanical Engineering Science*, vol. 230, pp. 1978–1986, 7 2016.
- [17] "Build one." [Online]. Available: <https://hapkit.stanford.edu/build.html>
- [18] M. O. Martinez, C. M. Nunez, T. Liao, T. K. Morimoto, and A. M. Okamura, "Evolution and analysis of hapkit: An open-source haptic device for educational applications," *IEEE transactions on haptics*, vol. 13, no. 2, pp. 354–367, 2019.
- [19] O. Baser and E. I. Konukseven, "Kinematic calibration of a 7 dof haptic device," in *2011 15th International Conference on Advanced Robotics (ICAR)*. IEEE, 2011, pp. 217–222.
- [20] "pyFirmata," 03 2019. [Online]. Available: <https://pypi.org/project/pyFirmata/>

- [21] "Load Cell Amplifier HX711 Breakout Hookup Guide - learn.sparkfun.com," 2022. [Online]. Available: <https://learn.sparkfun.com/tutorials/load-cell-amplifier-hx711-breakout-hookup-guide/installing-the-hx711-arduino-library-and-examples>
- [22] M. Hosseini, R. Meattini, G. Palli, and C. Melchiorri, "A wearable robotic device based on twisted string actuation for rehabilitation and assistive applications," *Journal of Robotics*, vol. 2017, 2017.
- [23] C. Hancock, *Performance & Design of Direct Current Machines*. CBS Publishers & Distributors, 2004. [Online]. Available: <https://books.google.nl/books?id=RVFIPgAACAAJ>

APPENDIX A

CALCULATION OF WEIGHT BENEFIT

This appendix supplies the calculation behind the potential weight saving when using a hybrid setup as opposed to using a DC motor.

The brake used in the prototype is a SenseGlove proprietary electromagnetic brake weighing 27 grams and running on a maximum voltage of 8 V. At 8 V the motor puts out a maximum force of approximately 2 N. In the prototype, voltage and the force generated by the motor share a linear correlation, see fig 22 on page 12. As such, the motor should put out a maximum force of approximately 12 N on the end effector at its maximum operating voltage of 48 V.

According to Hancock [23], the force generated by a DC motor is proportional to its volume. This claim is simplified greatly and leaves out complexities such as air gap flux density. However, when regarding a specific device, the Faulhaber 2342s048C motor in this case, the simplification is justified as all the variables like materials used are not changed. Following this theory, the motor could be down scaled 6 fold and still generate the same maximum force of 2 N. Theoretically, as the Faulhaber motor weighs 88 grams, this would result in a potential weight of 15 grams, see appendix C.2 on page 24. Of course this is much more nuanced in practice. Therefore, this calculation serves merely as indication. The combination would then weigh 42 grams in total. This does not take into account additional transmission or coupling needed, however if mounted on the same shaft, this would be an insignificant increase in weight.

The combined system would be capable of generating roughly 15 N of force with the brake active, see fig 23 on page 12, and approximately 2 N with the motor active, see fig 22 on page 12. However, a weight gain of 35 grams would be realised per actuator when comparing it with the mounted Faulhaber motor. If no motors exist with similar specification, it should be possible to build a custom DC motor.

APPENDIX B

HYBRID ACTUATOR FORCE DISCREPANCY

This appendix further elaborates on the principle of force discrepancy as introduced in this thesis. Force discrepancy is a phenomenon caused by the drivetrain non linearity due to using two different actuators. Using two actuators with

different capacity in series means that they will not be active simultaneously, inducing a certain force discrepancy when switching between the two actuators. This discrepancy occurs when the demanded force output exceeds the limit of one of the actuators and logically correlates positively with the growing of the demanded force. When simulating a spring with a linear stiffness and switching between the actuators whenever the motion direction switches, just like in the prototype, this becomes quite apparent.

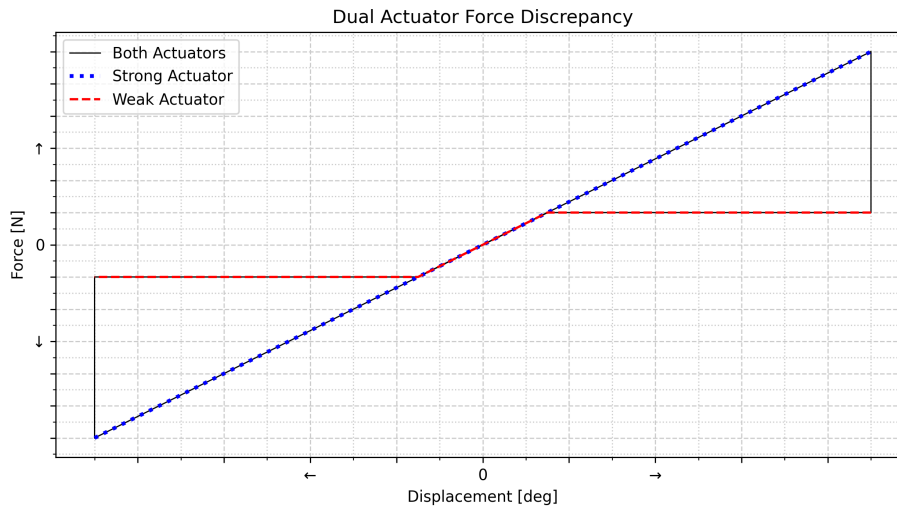


Fig. (31) Plots indicating the obtained force discrepancy upon use of two actuators with different maximum force outputs. The total force to displacement curve for any arbitrary double actuator system is shown in black. The dotted blue curve indicates the activity of the stronger actuator and the dashed red curve indicates the activity of the weaker actuator

The force displacement curve of an ideal linear stiffness would look like a straight diagonal line. However, due to using two actuators, a discrepancy is introduced whenever the direction of motion changes. This causes the diagonal line to change into a bow tie shape. As can be observed in fig 31. Due to one of the actuators being weaker than the other, upon change of motion direction the actuator activity switches and the force drops when changing from the stronger to the weaker motor, the opposite happens on the other side of the figure, these force changes can be observed in the figure as the vertical black lines.

APPENDIX C

SUPPLEMENTARY DOCUMENTS

C.1 Collection of Code

All the code used throughout the thesis; to control the prototype, generate data, visualize the data and lastly analyse the data can be found in: [SAvGinneken - Thesis Material](#)

C.2 Electrical Components

Data sheets of the used electrical components can be found in: [SAvGinneken - Thesis Material](#)

APPENDIX D

PROTOTYPE ACTUATOR CHARACTERISTICS

The cloud drive supplied in appendix C.1 on the preceding page includes the code used to generate the actuator characteristics figures as in 4.2 on page 10.

To get the correct force (at the end effector) to voltage relation of the Faulhaber DC motor as used in the prototype. The end effector is locked in place so it cannot move under operation of the DC motor. The force at the end effector was measured for 15 iterations of continuous 0 to 16 to 0V actuator voltage. The captured data is plotted against the voltage and the result is fig 22 on page 12. Through this data a first order polynomial was fitted via regression resulting in the motor characteristic function as in fig 22 on page 12. To find the brake characteristics 30 iterations of continuous 1 to 16V actuator voltage were performed and plotted, again a first order polynomial was fitted via regression resulting in fig 23 on page 12. It was found that for voltages lower than 1V the brake does not engage, hence the characteristic was calculated for the range of 1 – 16V, for the 0 – 1V the actuator output is generalized to 0N. Again, a first order polynomial is fitted to generate the brake characteristic function as in fig 23 on page 12

APPENDIX E CONTROL SEQUENCE

Schematic visualisation of the data flow during the control sequence.

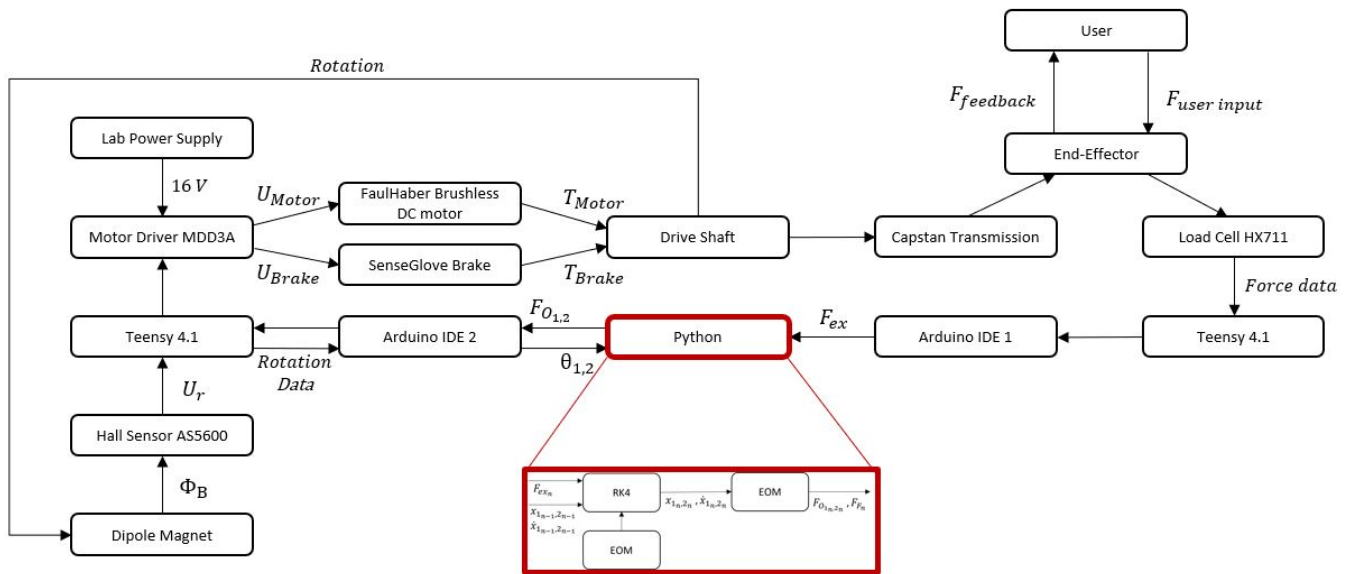


Fig. (32) Control sequence diagram indicating the data flow of the prototype when in use

APPENDIX F SIMULATION RESULTS

Supplied are the simulation results when the model is fed with the step and ramp input as provided in 2 on page 4. They are supplied both with and without the added finger interaction.

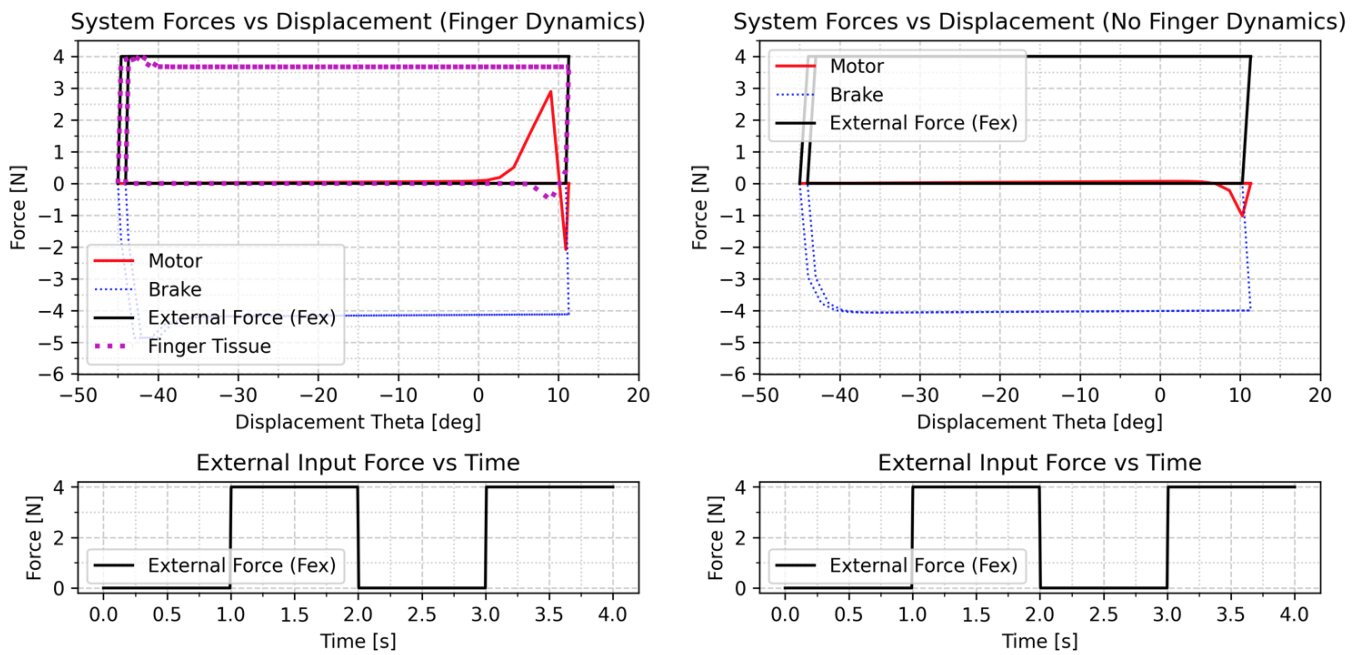


Fig. (33) Visualization of the simulation model fed with the step input as in 8 on page 6, both with and without finger dynamics

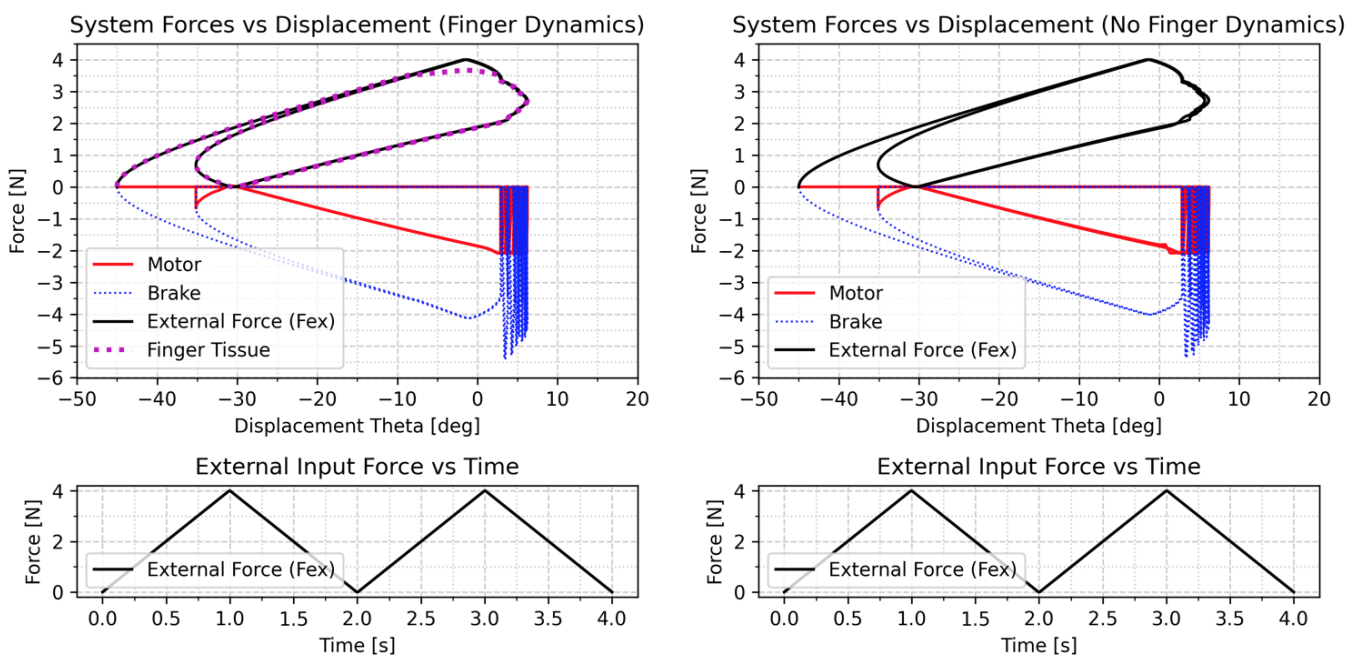


Fig. (34) Visualization of the simulation model fed with the ramp input as in 8 on page 6, both with and without finger dynamics

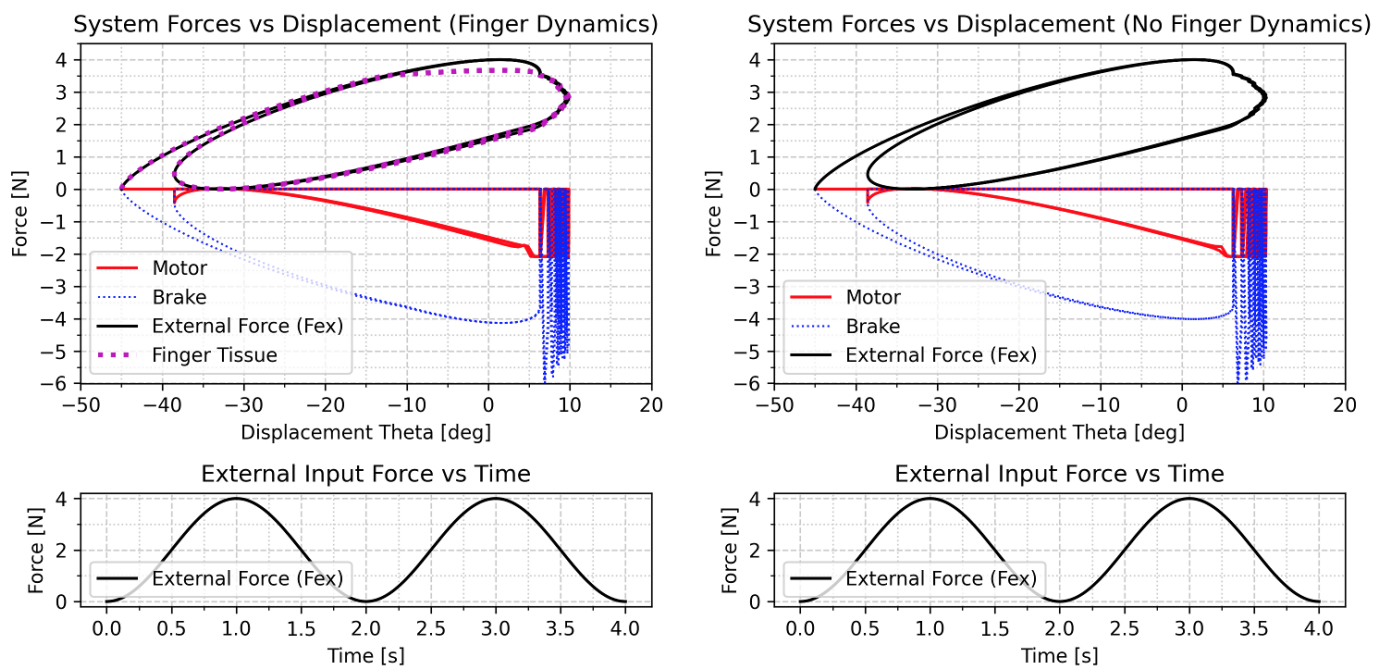


Fig. (35) Visualization of the simulation model fed with the sinusoidal input as in 8 on page 6, both with and without finger dynamics

APPENDIX G
EXPERIMENT RESULTS

Find all test runs gathered in the 6 figures below. Each figure shows the 6 test runs of each actuation method and modelled environment combination. Additional plots of each separate trial and the raw data can be found in: [SAvGinneken - Thesis Material](#)

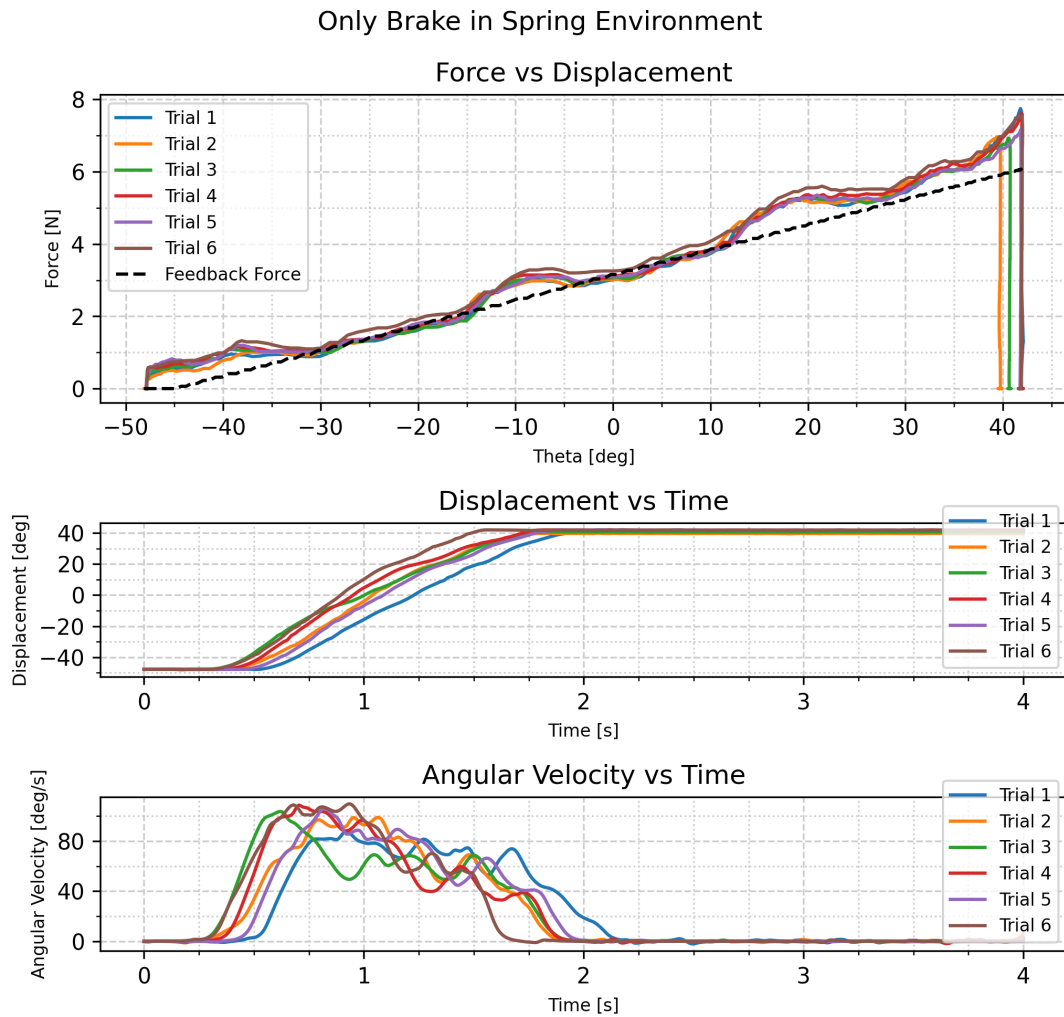


Fig. (36) This figure shows the results of the 6 test runs using the passive actuation method in the spring environment. It includes a force vs displacement, displacement vs time and a angular velocity vs time plot. The dotted black line is the feedback force as sent to the actuator, calculate from the actuator characteristics and the input voltage

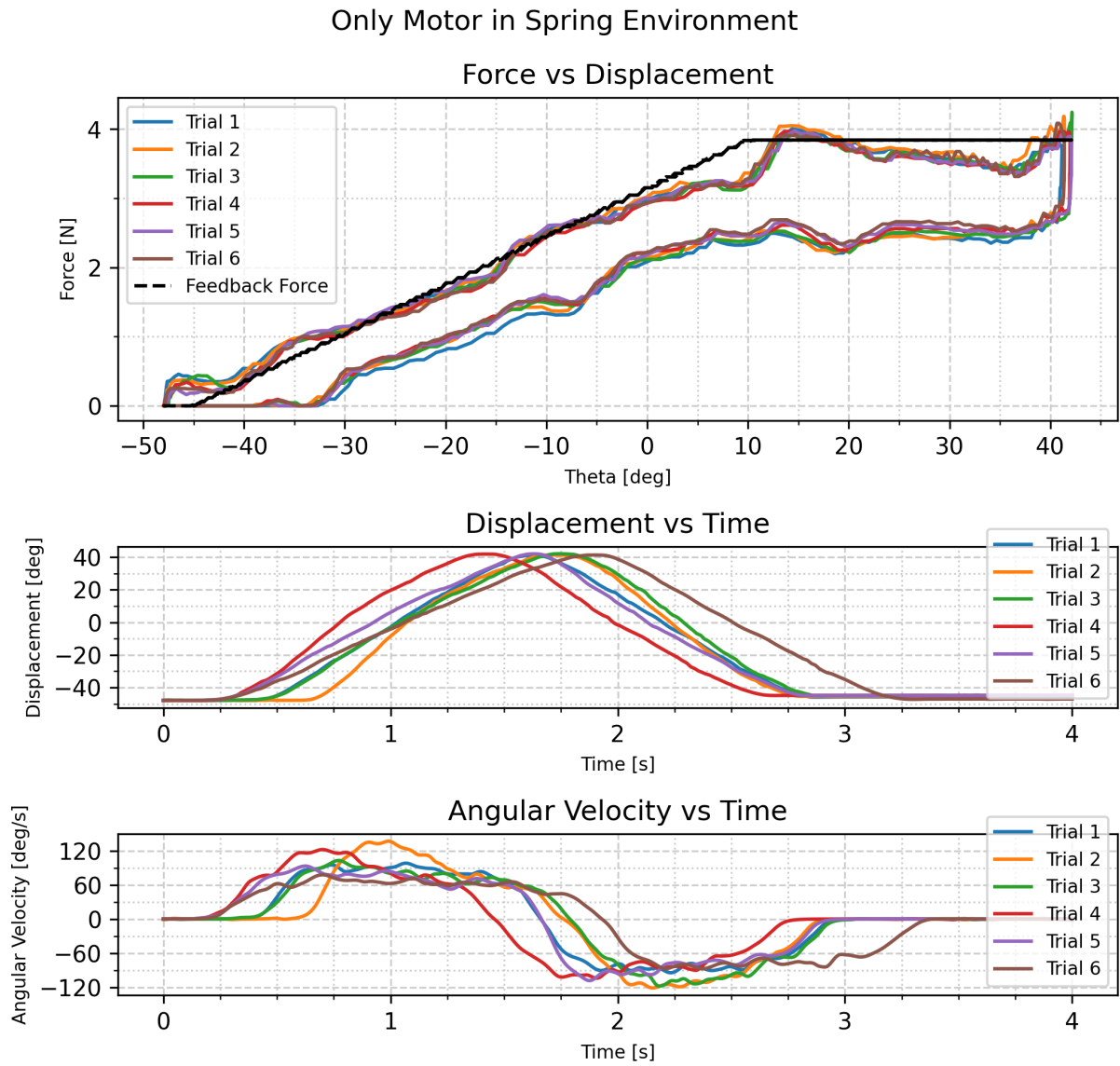


Fig. (37) This figure shows the results of the 6 test runs using the active actuation method in the spring environment. It includes a force vs displacement, displacement vs time and a angular velocity vs time plot. The dotted black line is the feedback force as sent to the actuator, calculate from the actuator characteristics and the input voltage

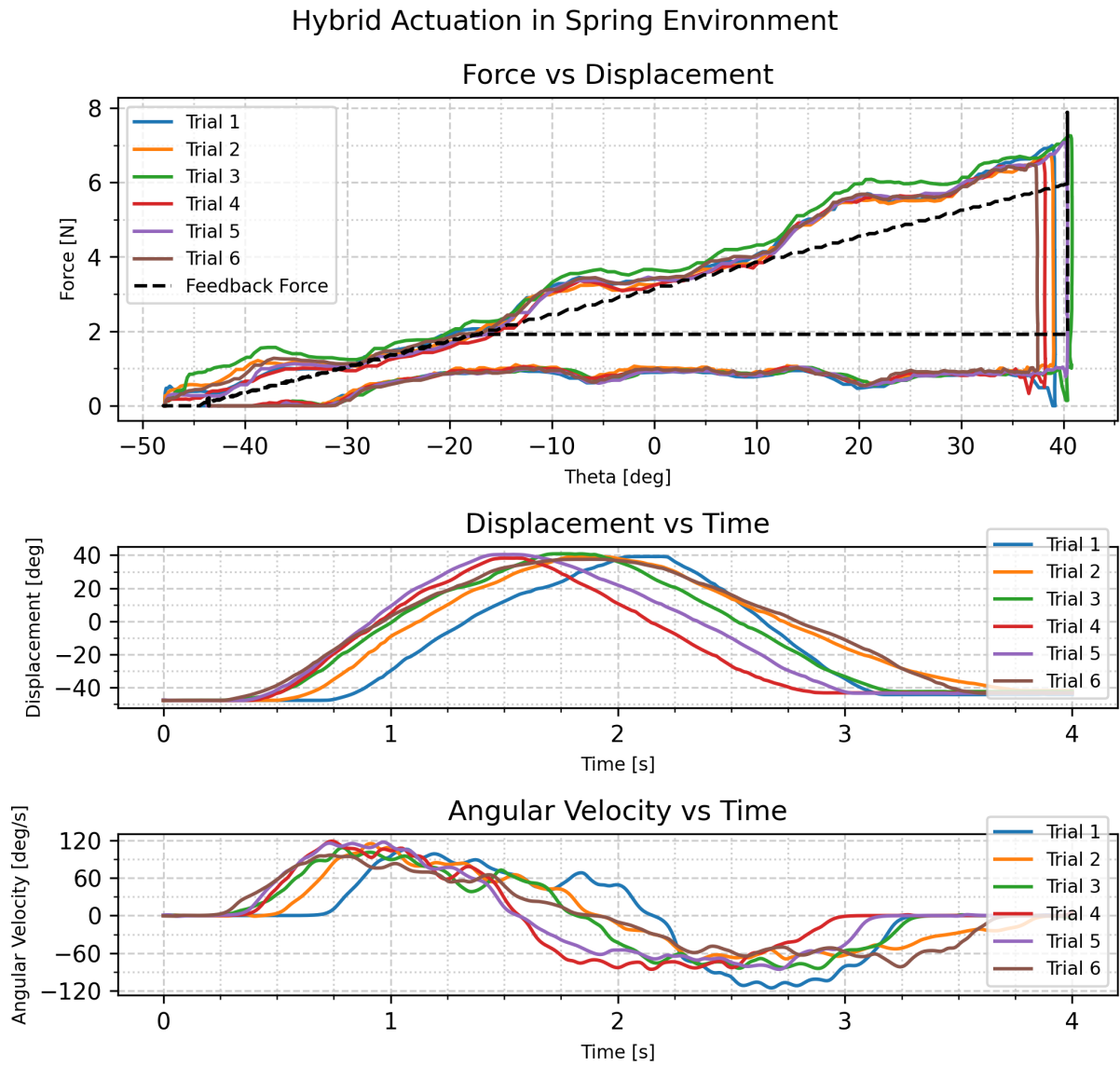


Fig. (38) This figure shows the results of the 6 test runs using the hybrid actuation method in the spring environment. It includes a force vs displacement, displacement vs time and a angular velocity vs time plot. The dotted black line is the feedback force as sent to the actuator, calculate from the actuator characteristics and the input voltage

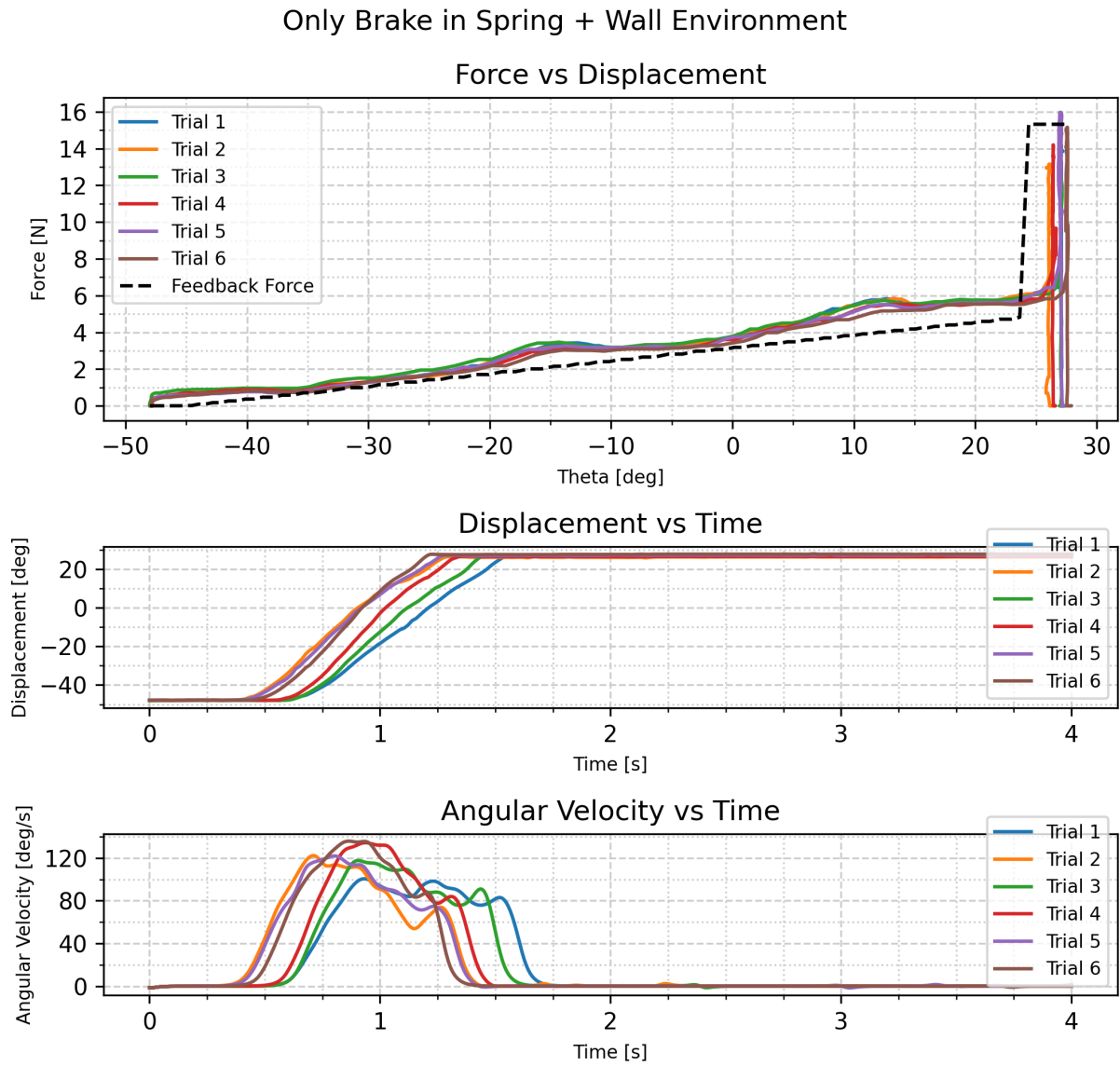


Fig. (39) This figure shows the results of the 6 test runs using the passive actuation method in the spring + wall environment. It includes a force vs displacement, displacement vs time and a angular velocity vs time plot. The dotted black line is the feedback force as sent to the actuator, calculate from the actuator characteristics and the input voltage

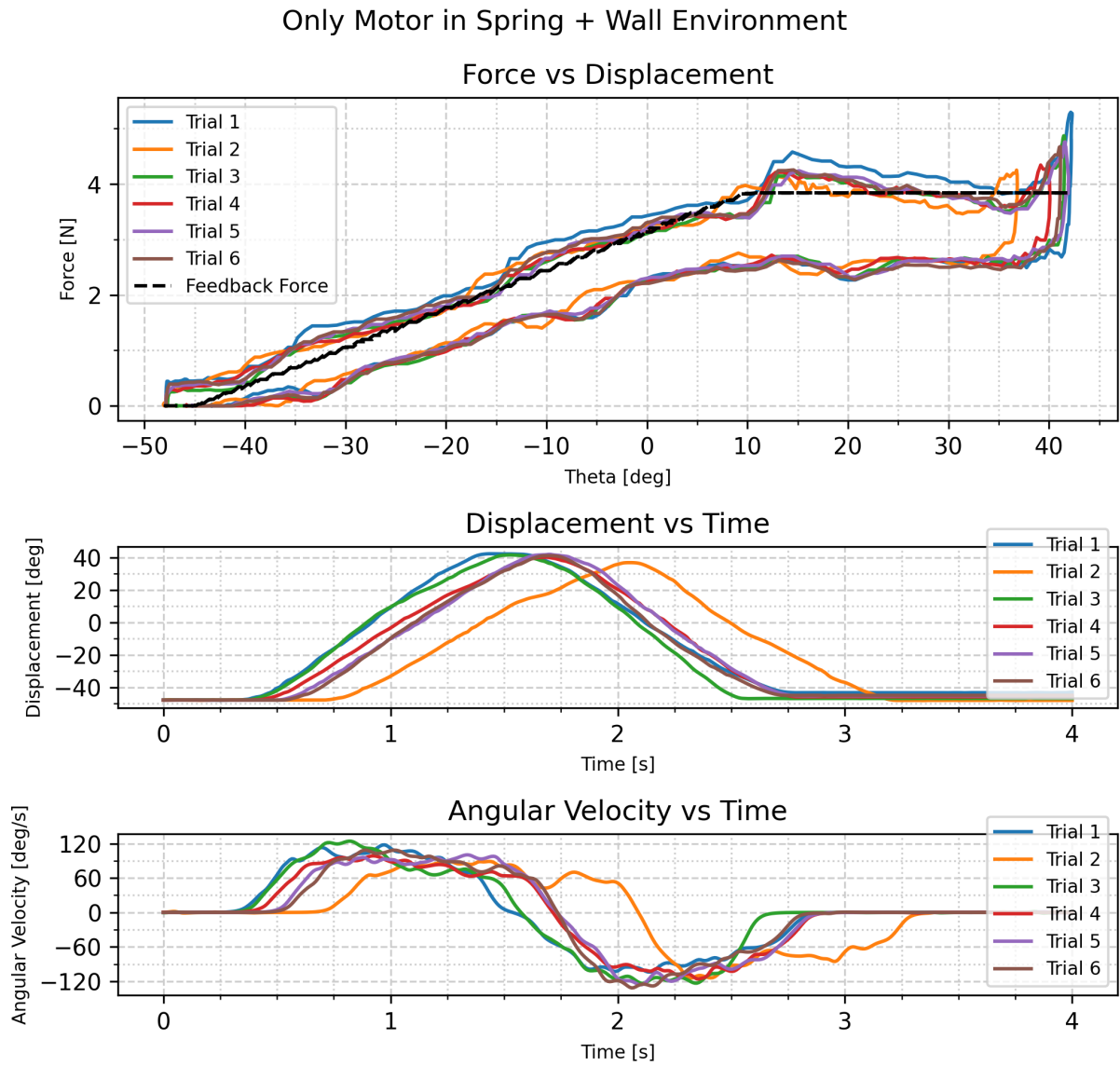


Fig. (40) This figure shows the results of the 6 test runs using the active actuation method in the spring + wall environment. It includes a force vs displacement, displacement vs time and a angular velocity vs time plot. The dotted black line is the feedback force as sent to the actuator, calculate from the actuator characteristics and the input voltage

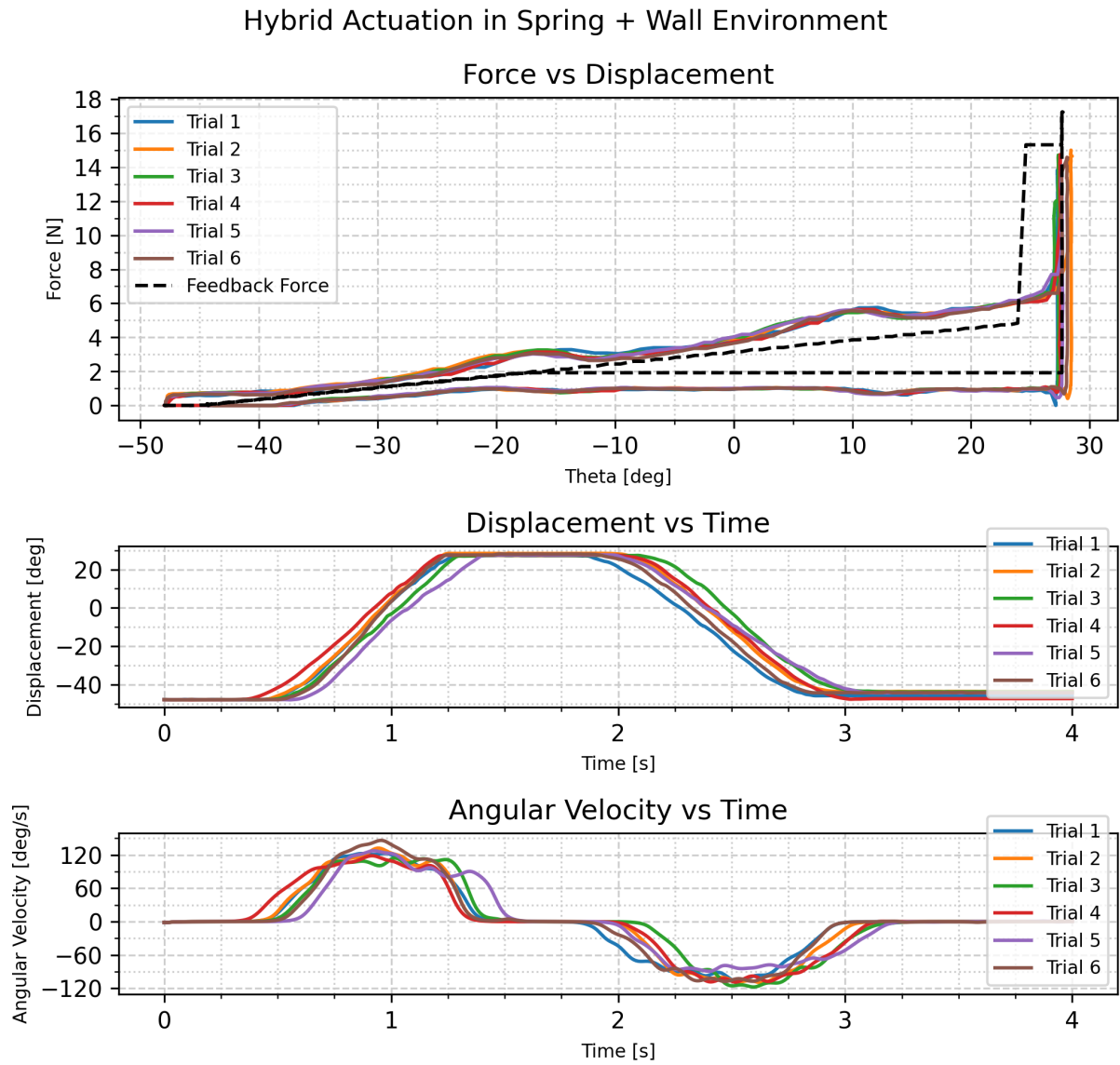


Fig. (41) This figure shows the results of the 6 test runs using the hybrid actuation method in the spring + wall environment. It includes a force vs displacement, displacement vs time and a angular velocity vs time plot. The dotted black line is the feedback force as sent to the actuator, calculate from the actuator characteristics and the input voltage